Thermal Lensing in a High Power Diode-Pumped Continuous Wave Yb^{+3}:$KY(WO_4)_2$ Laser

by

Hamidreza Mirzaeian

A Thesis submitted to the Faculty of Graduate Studies of

The University of Manitoba

in partial fulfillment of the requirements of the degree of

MASTER OF SCIENCE

Department of Electrical and Computer Engineering

University of Manitoba

Winnipeg

Abstract

High power diode-pumped solid state (DPSS) lasers are a rapidly growing technology that is attractive for various applications in scientific and industrial fields. DPSS lasers are highly efficient, reliable and durable with superior beam quality when compared to flash-lamp pumped lasers. Double-tungstate crystals such as potassium yttrium tungstate Yb:$KY(WO_4)_2$ (Yb:KYW) are one of the most popular active materials used in DPSS lasers for generation of continuous wave radiation and ultrashort (i.e. femtosecond, 10^{-15} s) pulses with high average output power. The high pump power of laser diodes results in considerable heat generation in a laser crystal that in turn causes thermal lensing effect. Thermal lensing affects the performance and stability of a resonator, and plays an important role in limiting the output power and degrading the beam quality of solid state lasers. Despite these facts, no detailed studies of thermal effects in Yb:KYW lasers were reported to date. In this work thermal lensing in a diode-pumped Ng-cut Yb:KYW laser operating at the wavelength of 1.04 μm was characterized. A maximum output power of 3.5 W with a nearly diffraction limited output beam ($M^2 < 1.2$) was achieved under the absorbed pump power of 13.8 W. The focal lengths of the induced thermal lenses were obtained from the laser output beam size measurements at various incident pump power levels and ABCD matrix analysis. At maximum output power the focal length of the induced thermal lens was found to be 814 mm for the N_m direction (horizontal) and 144 mm for the N_p direction (vertical). Thermal lens sensitivity factors were 1.26 m^{-1}/W and 0.32 m^{-1}/W for the N_p and N_m directions, respectively. This highly astigmatic thermal lensing can be explained by strong anisotropy of thermo-optical properties of the crystal and its cooling geometry. In addition, the finite element analysis (FEA) method was

employed to obtain the focal lengths of the induced thermal lens inside the crystal. Simulation results obtained from the theoretical model were compared to experimental data, and the accuracy of the model was verified. The results of this work are critical for practical design of the efficient and reliable Yb:KYW lasers with multi-Watt average output power.

Acknowledgements

First and foremost, my deepest gratitude is to my advisor, Prof. Arkady Major. His support and guidance helped me in every step of my studies and writing of this thesis. I am deeply and forever indebted to you for giving me the opportunity to work under your guidance.

I would also like to thank the members of my committee, Prof. Cyrus Shafai and Prof. Andrew L. Goertzen for taking the time to review my thesis and participate in my defense.

I especially want to thank my friends and fellow graduate students Sujith Manjooran and Haitao Zhao for their help, comments and suggestions throughout the entire thesis process.

I would also thank my loved ones, my family and specially my dear niece Sara.

Table of Contents

List of Figures

List of Tables

Chapter 1

1.1 Introduction

The first laser was demonstrated in 1960 and was based on ruby. Since then, lasers have been used in many diverse applications in medical, scientific and industrial fields. High intensity, high directionality, and high degree of coherence and polarization are some of the unique properties of laser radiation. Moreover, solid state lasers and especially diode-pumped solid state lasers (DPSSL) are highly efficient, reliable and durable with superior beam quality when compared to flash-lamp pumped lasers. However, in the early stages of development of high power lasers and before the development of high brightness InGaAs laser diodes, flash-lamp pumping was the main method of choice. As a result neodymium (Nd) doped gain media were preferred over ytterbium (Yb) gain media mainly due to their suitability for flash-lamp pumping. Although coherent oscillation from the Yb^{3+} ion was first demonstrated in 1965 in Yttrium Aluminium Garnet (YAG) [1], the use of Yb^{3+} ion as a dopant in laser crystals was mainly ignored until the early 1990's. In the last two decades the InGaAs laser diodes became available to match the particular pump transitions of Yb^{3+} doped laser crystals [2], and Yb-doped lasers are gradually replacing Nd-doped lasers. Potassium yttrium tungstate $Yb:KY(WO_4)_2$ (Yb:KYW) is one of the most popular active materials used in DPSS lasers for generation of continuous wave radiation and ultrashort (i.e. femtosecond, 10^{-15} s) pulses with high average output power. The high pump power of laser diodes results in considerable heat generation in a laser crystal that in turn causes thermal lensing effect. Thermal lensing affects the performance and stability of a resonator, and plays an important role in limiting the output power and degrading the beam quality of solid state lasers. Theoretical investigation on thermal lensing effects of Yb:KYW has been performed previously [3]; however, no experimental studies of thermal lensing effect in Yb:KYW lasers were reported to date. The aim of this master's thesis project was to conduct detailed

experimental studies into thermal lensing in Yb:KYW laser for the first time. This study and the results of this work are important for practical design of efficient and reliable multi-Watt Yb:KYW lasers.

Chapter 2

Thermal Lensing and Laser Cavity Design

2.1 Heat generation in laser crystal

Several reasons contribute to the generation of heat in solid state lasers. The energy difference between the pump band and the upper laser level, and the energy difference between the lower laser level and the ground state is lost and converted to heat. This photon energy difference is called quantum defect and it can be estimated by the equation:

$$q = \left(1 - \frac{\lambda_{Pump}}{\lambda_{Laser}}\right) * 100\ \% \quad (1)$$

In Yb:KYW the peak absorption is at 981.2 nm and lasing occurs around 1.04 μm; therefore, the quantum defect of Yb:KYW is usually very low (<6%). A quantum defect as low as 0.6 % was reported corresponding to a laser operation at 987 nm [4]. Quantum defect is the major source of heating in solid-state lasers, and the low quantum defect in Yb:KYW lasers results in lower heat generation.

Additionally, radiative quantum efficiency for the upper and lower manifolds in Yb:KYW can be less than unity. Nonradiative transitions can occur due to multi-phonon transitions and concentration quenching which result in additional heat generation inside the gain medium.

2.2 Thermal lensing theory

Yb:KYW has moderate thermal conductivity of around 3 $Wm^{-1}K^{-1}$. This results in high temperature gradient inside the crystal. The transverse temperature gradient results in change of refractive index inside the crystal through the thermo-optic effect. Additionally, temperature gradient inside crystal leads to a thermally induced mechanical stress. The induced mechanical stress causes further changes in refractive index through photo-elastic effect. Moreover, thermally induced mechanical stress results in bulging of the end faces of the crystal, and in extreme cases could result in crystal fracture. Bulging and induced refractive index gradient results in lensing effect which is called thermal lensing. Thermal lensing results in the degradation of laser output beam quality and a mismatch between the cavity and pump modes, which in turn leads to lower cavity stability, reabsorption at laser wavelength, and even unstable cavity in extreme cases.

In general the three effects that contribute to thermal lensing in lasers are:

1- The temperature dependence of refractive index which is described by thermo-optic coefficient of the crystal dn/dT. The thermo-optic coefficient dn/dT of Yb:KYW has been studied by several research groups (see section 2.5 in Chapter 2) .

2- The endface deformation and bulging of the crystal caused by the thermally induced mechanical expansion. The bulging effect is characterized by longitudinal thermal expansion coefficient of the crystal α. Thermal expansion values of Yb:KYW have also been studied and reported (see section 2.5 in Chapter 2).

3- Changes of the refractive index caused by the thermally induced stress through the photoelastic effect.

As a summary, a schematic diagram showing the thermal lensing process in solid state lasers is presented in Fig. 1.

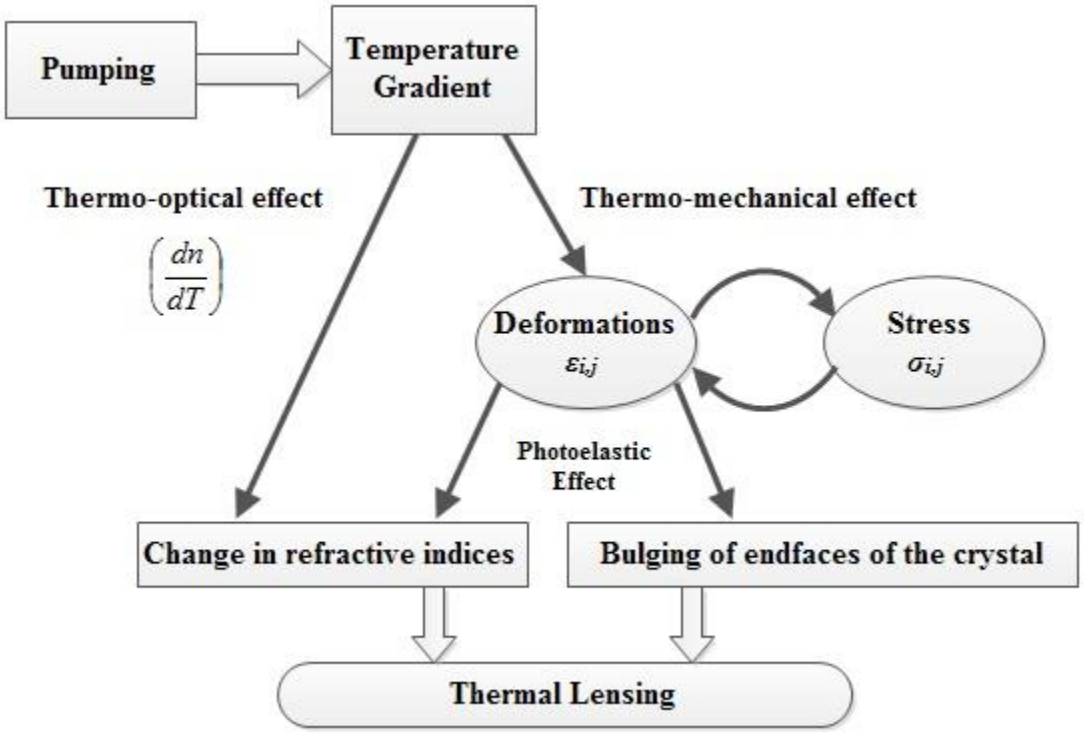

Figure 1: Summary of effects causing thermal lens in solid state lasers

In general, the change of the refractive indices by temperature gradient can be described by:

$$n(x,y,z) = n_0(x,y,z) + \Delta n_T(x,y,z) + \Delta n_\varepsilon(x,y,z) \tag{2}$$

where n_0 is the initial value of the refractive index and Δn_T and Δn_ε are the temperature and stress induced changes of it. The change in refractive indices combined with deformation of the crystal result in distortion of a laser beam and can be described by a thin lens. A temperature distribution inside the crystal should be known in order to

calculate the effect of thermal lensing. The temperature distribution inside the crystal is described by the heat diffusion equation [5]:

$$\nabla^2 T(x,y,z) = -\frac{q_{th}(x,y,z)}{K_c(T)} \tag{3}$$

where $q_{th}(x,y,z)$ is the heat source density inside the crystal, and K_c is the thermal conductivity. Under approximations and simplifications such as symmetric top-hat pump profile, constant thermal conductivity and using rod-shaped isotropic gain medium, Eq. 3 can be solved analytically. In more complicated cases finite element analysis (FEA) method can be used for numerical solutions.

2.3 Thermal lensing measurement techniques

Power scaling of diode pumped solid state lasers is one of the main issues in designing lasers. High power laser diodes are rapidly developing and diode pumped solid state lasers are offering high efficiency together with high power. However end-pumping with high intensities creates thermal problems which in turn limits the power scaling. Thermal lensing affects the performance and stability of the resonator, and it should be well understood and studied before designing of a high power laser. The chosen thermal lensing measurement technique should be suitable for end-pumped geometries such that characterization could be done under lasing action.

A variety of measurement techniques for thermal lensing have been developed and presented in different literatures. In the following sections some of the methods are briefly explained.

2.3.1 Passing a probe beam

One method to measure thermal lens is to pass a probe beam with the same dimension as the laser beam through the active medium and to study its deflection, defocussing or intensity.

The intensity of a probe beam can be measured through a slit after it passes the laser crystal as it is shown in Fig. 2. When the laser crystal is not pumped, the intensity profile of the probe beam is determined. This intensity profile can then be compared to the case where the laser crystal is pumped and thermal lensing effect is present. When the focal length of the thermally induced lens within the crystal is shorter than the distance between the crystal and the slit, the radius of the beam will be greater than the width of the slit and the probe beam will get attenuated. When the focal length of the induced lens is greater than the distance between the crystal and the slit, the probe beam will pass the slit with less attenuation. This technique is not suitable for determining very long or very short focal lengths, since in both cases the probe beam will get attenuated. Also if the probe beam is larger than the excited area in the crystal, then only a part of the beam will experience the thermal lens which can cause error in measurement.

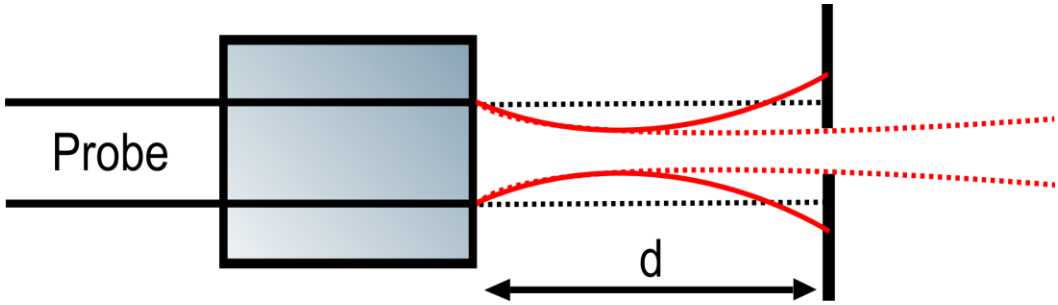

Figure 2: Thermal lens measurement based on intensity profile through a slit

The thermal lens could also be evaluated by passing a probe beam through a pumped crystal and measuring the divergence or the beam diameter of the probe beam. It should be noted that lensing effect is different under lasing action and nonlasing action; therefore, these methods can give inaccurate results.

The thermal lens could also be measured by detecting the deflection of a probe beam by the induced thermal lens. In this method a small off-axis beam is incident on the pumped crystal, and deviation of the beam will be measured using a detector. The probe beam

will be deflected towards the axis for converging (positive) thermal lens and away from the axis for diverging (negative) thermal lens. This method is complex and only used in determining the focal length of the laser under transverse pumping.

2.3.2 Studying cavity stability regions

Thermal lensing effect can make cavity unstable. By using a simple plane-parallel cavity with intra cavity lens and monitoring the output power, the stability range of the laser can be obtained. ABCD matrix analysis can also be used to find the focal lengths of the thermal lens over which the cavity is stable. By comparing these two steps the focal length of the thermal lens can be estimated. These methods are relatively easy to implement since a probe beam is not needed and the laser output power is used to measure the thermal lens.

2.3.3 Characterizing beam with wavefront sensor

A wavefront sensor can be used to determine the focal length of the induced thermal lens. An example of this method is Shack-Hartmann wavefront sensing. Shack-Hartmann wavefront sensor is able to measure the aberrations of an optical wavefront. The sensor is made of a lens array of the same focal length to split the incident light which is then focused onto a CCD camera. The aberrations of wavefront across each micro-lens can then be detected from the position of the focal spot on the CCD camera. This technique can be employed by measuring the wavefront of a reference beam when pump is turned off and then comparing it to the distorted wavefront when pump is turned on. As a result the phase distortions due to thermal effects can be recorded and the focal lengths of the thermal lens can be measured.

2.3.4 Beam width measurement and ABCD modeling

ABCD matrix analysis can be used to calculate the beam radius at the output coupler of a laser cavity. By calculating the beam radius at the output coupler with added lens element (thermal lensing can be modeled as a thin lens inside the crystal) and comparing the

calculated value to the experimentally measured beam radius, the focal length of the induced thermal lens can be estimated. It is this method that was employed in our study of thermal lensing. ABCD matrix analysis can also be applied under nonlasing condition where a probe beam is passed through a pumped laser crystal. By measuring the dimension of the probe beam as it propagates and comparing the measured values to the calculated ABCD matrix analysis, the thermal lens can be estimated.

2.3.5 Interferometric techniques

Different interferometric techniques such as Michelson [6], Mach-Zehnder [7], Twyman-Green [8] and lateral shear [9] have been used to study thermal lensing in lasers. In interferometric techniques, generally a probe beam is passed through a laser crystal and is compared with a reference beam. The phase difference between the two beams is due to changes in optical path length. This phase difference is usually recorded in the form of fringe patterns and is used to determine the distortion to the wavefront of the probe beam as it passes the induced thermal lens. These methods are usually not suitable for end-pumped lasers due to the small spot size of the pumped region in the crystal. When the pumped region is much smaller than the probe size, the interference patterns will be small, and it will be difficult to resolve them.

2.4 Laser cavity design

In a laser cavity, laser radiation circulates and passes through the gain medium. This circulation compensates for the losses introduced within the cavity by different elements, including an output mirror with partial transmission. Solid state lasers are usually constructed with several mirrors and a laser crystal as the gain medium. One of the most important criteria in designing a laser cavity is matching of a laser beam radius inside the gain medium to the radius of the pumped region. Other criteria such as effect of thermal lensing on mode sizes, stability and beam quality over a wide range of pump powers are

critical in designing high power solid state lasers. Factors such as low sensitivity to misalignment, minimizing round-trip losses, the number of optical components and overall compactness of the cavity is also considered in designing of solid state lasers.

2.4.1 ABCD law

In order to build a laser, a cavity should be designed and simulated using an ABCD matrix analysis. Using this technique, the precise distances between the cavity elements can be calculated. An ABCD matrix is a 2×2 matrix that characterizes an optical element and describes the effect of an element on a laser beam. ABCD matrix analysis can be used to design a cavity with the required spot sizes, and to verify the stability against changes in the length of the cavity arms. The transfer matrices of different cavity elements are given by:

$$\begin{cases} Flat\ Mirror = \begin{bmatrix} 1 & 0 \\ 0 & 1 \end{bmatrix} & Curved\ Mirror\ = \begin{bmatrix} 1 & 0 \\ -2/R & 1 \end{bmatrix} \\ Free\ Space\ Propagation = \begin{bmatrix} 1 & L \\ 0 & 1 \end{bmatrix} & Crystal = \begin{bmatrix} 1 & d/n \\ 0 & 1 \end{bmatrix} \end{cases} \quad (4)$$

where R is the radius of curvature of the mirror, L is the distance of free space, d is the length of the crystal and n represents the refractive index of the crystal.

Lens equivalent waveguide of a Z-cavity is illustrated in Fig. 3 where curved mirrors are replaced by the equivalent lens elements for the purpose of ABCD matrix analysis.

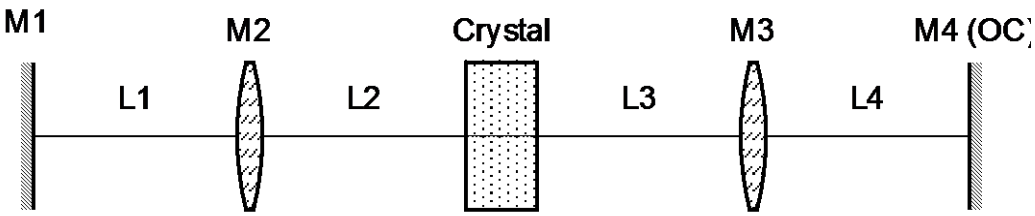

Figure 3: Lens equivalent waveguide

The cavity propagation matrix is created by multiplying the transfer matrix for each element and is given by:

$$M_T = \begin{bmatrix} A & B \\ C & D \end{bmatrix} \tag{5}$$

A cavity propagation matrix at the position of the crystal for the Z-cavity in Fig. 3 is given by:

$$M_T = C_r * d_2 * M_2 * d_1 * M_1 * d_1 * M_2 * d_2 * C_r * d_3 * M_3 * d_4 * M_4 * d_4 * M_3 * d_3 \tag{6}$$

The complex q parameter of a Gaussian beam which is related to the beam radius w and the wavefront curvature R by:

$$\frac{1}{q} = \frac{1}{R} - i\frac{\lambda}{\pi w^2} \tag{7}$$

A transformation of a Gaussian beam as it passes through an optical system is given by:

$$q_2 = \frac{Aq_1 + B}{Cq_1 + D} \tag{8}$$

In a stable cavity the beam repeats itself after one cavity roundtrip; therefore, the beam radius and wavefront curvature should stay the same at each particular element within the cavity. By contrast, in an unstable cavity the beam does not replicate itself and it will not be confined within the cavity. In order to have a stable cavity the following condition should be satisfied:

$$q_1(z) = \frac{Aq_1(z) + B}{Cq_1(z) + D} \tag{9}$$

The beam parameter q is the function of position z within the cavity and the corresponding propagation matrix M_T is obtained by multiplying the transfer matrices of each element within the cavity roundtrip starting and finishing at the same position. The beam radius can then be found by solving Eq. 9 and comparing it to Eq. 7:

$$w^2 = \frac{\lambda|B|/\pi}{\sqrt{1-(D+A)^2/4}} \tag{10}$$

The wavefront curvature can be found to be:

$$R = \frac{2B}{D-A} \tag{11}$$

In order to have a stable cavity w should be positive and real which implies:

$$\left(\frac{A+D}{2}\right)^2 \leq 1 \quad \Rightarrow \quad -1 \leq \left(\frac{A+D}{2}\right) \leq 1 \tag{12}$$

In a stable cavity, condition in Eq. 12 must be satisfied for all positions within the cavity. Therefore, by calculating the M_T at each position in the cavity the beam radius can be found. A stable cavity which supports the desired beam waists around the cavity can be designed by changing the separations and radius of curvature of the used mirrors. The matrix element C from the propagation matrix M_T can be used to study the sensitivity of the cavity to misalignments and to compare different cavity designs [10].

Chapter 3

Background

3.1 Ytterbium ion

Ytterbium with symbol Yb is the 13^{th} chemical element in the set of fourteen trivalent rare earth ions. It is one of the most important rare earth ions used in lasers' gain medium.

Yb^{3+} cation electronic configuration is given by Xenon $4f^{13}$ with lack of one electron to completely fill its valance shell. In the Yb^{3+} ion, the 4f shell is shielded by 5s and 5p shells which results in reduced effect of host lattice on cross sections of optical transitions. Yb^{3+} ion has only two manifolds, the ground state $^2F_{7/2}$ and the excited state $^2F_{5/2}$ with the approximate separation of 10,000 cm^{-1} [11]. This separation corresponds to emission and absorption of about 1 micron depending on the host, temperature, and the Stark levels involved [12]. Due to this very simple two manifold energy scheme, losses such as excited-state absorption, upconversion and concentration quenching are absent in Yb^{3+} doped gain medium [13].

There is a wide variety of laser crystals which can act as a host for Yb^{3+} ion and result in broad emission bandwidths suitable for ultrashort pulse generation [14]. Ytterbium doped glasses are also used in high power fiber amplifiers [15] and fiber lasers [16, 17]. In order to increase the absorption efficiency, ytterbium is used in erbium doped fibers as a sensitizer to increase the pump absorption and the transfer of energy to erbium ions [18].

3.2 Double tungstates

A suitable choice of host material is a significant factor in obtaining a good gain medium with desirable laser performance. Crystalline hosts despite their high fabrication costs compared to glasses have many advantages such as high thermal conductivity, large emission and absorption cross sections, and even relatively broad emission bandwidth. Double tungstates also have a high Raman gain coefficient which is favorable for generating additional laser wavelengths due to self-Raman conversion [19]. They are good candidates for generating ultrashort pulses due to their broad emission bandwidths. In recent years double tungstate crystals such as $KY(WO_4)_2$ (KYW), $KGd(WO_4)_2$ (KGdW) and $KLu(WO_4)_2$ (KLuW) started to attract a lot of attention due to their excellent optical properties when used in solid state lasers. Double tungstates are used as host crystals with various rare earth dopants such as Nd^{3+}, Er^{3+}, Tm^{3+} and Yb^{3+}.

3.3 Crystal structure of $KY(WO_4)_2$

The first laser based on Potassium Yttrium Tungstate $KY(WO_4)_2$ crystal activated with Nd^{3+} ions was demonstrated more than forty years ago [20]. $KY(WO_4)_2$ is a monoclinic crystal which can be described by both $C2/_c$ and $I2/_c$ space groups. The crystallographic axes *a*, *b* and *c* in $I2/_c$ space groups notations, and the relative direction of the three orthogonal refractive index axes N_m, N_p and N_g are illustrated in Fig. 4 [21].

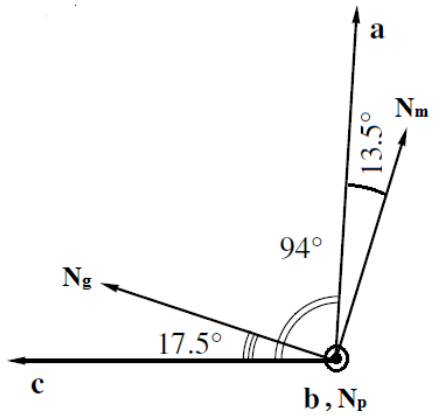

Figure 4: The relation between crystallographic and refractive index axes in $KY(WO_4)_2$

Unit cell parameters of $KY(WO_4)_2$ crystal are shown in Table 1 [21].

Table 1. Unit cell parameters of $KY(WO_4)_2$

	Unit Cell Parameters			
KYW	***a***	***b***	***c***	***β***
	8.05	10.35	7.54	94
	a^*	b^*	c^*	β^*
	10.64	10.35	7.54	130.5

The angle between crystallographic axis *a* and principal refractive index axis N_m is 13.5˚. N_g axis makes a 17.5˚ angle with *c*, and *b* is parallel to N_p.

3.4 Ytterbium doped potassium yttrium tungstate Yb^{3+}:$KY(WO_4)_2$

In Yb:KYW, the Yb^{3+} ion replaces yttrium. The ionic radii of Y^{3+} and Yb^{3+} are 90.0 pm and 86.8 pm respectively. Due to these similar ionic radii high doping concentrations of ytterbium can be achieved without concentration quenching with a good quality crystal. Ytterbium as an active ion in KYW results in strong absorption cross section around 980 nm which is suitable for diode pumping with InGaAs laser diodes. Diodes are compact,

efficient and can be tuned to match the exact absorption bands of the gain medium. Compared to Yb:YAG, the gain bandwidth of Yb:KYW is much larger which provides wide wavelength tunability and shorter pulses in the mode-locking regime. Furthermore, Yb:KYW possess a high emission cross section which is useful in the passive mode-locking in order to avoid Q-switching instabilities. Yb:KYW is most efficiently pumped at 981 nm and laser wavelength can be achieved below 1 μm [22] which results in a very small quantum defect and subsequent reduction in heat generation. Although thermal conductivity of Yb:KYW is about half that of Yb:YAG, this can be partly compensated by its relatively small quantum defect. Yb:KYW is naturally birefringent which eliminates thermally induced polarization rotation and subsequent depolarization loss.

3.5 Quasi-three-level system

Yb^{3+} ion doped lasers are considered as quasi-three-level lasers since the lower lasing level is thermally populated at room temperature. This lower level population results in reabsorption of a part of the emitted laser light. In order to overcome this reabsorption loss higher pumping intensities and good overlap between the pump mode and the cavity mode throughout the crystal length is required. The incident continuous wave laser threshold pump power can be estimated to be [23]:

$$P_{inc,th} = \frac{\pi h \nu_p \left(\omega_p^2 + \omega_m^2\right)}{4\eta_{pq}(\sigma_{em} + \sigma_{aL})\tau\left(1 - e^{-\alpha_c l_g}\right)}(T + L_{int} + 2\sigma_{aL}N_{ion}l_g) \qquad (13)$$

where ω_p and ω_m are the pump and cavity mode spot sizes in crystal, T is the output coupling and L_{int} represents the passive roundtrip losses such as scattering or Fresnel reflection from the crystal. The stimulated absorption and emission cross sections are σ_{aL} and σ_{em} at laser wavelength, l_g is the length of the gain medium, N_{ion} is the number of ions in lower lasing level, τ is the upper state lifetime, η_{pq} is the pump quantum

efficiency and α_c is the absorption coefficient at pump wavelength. It can be observed that low threshold power requires long upper state lifetime, low losses, small pump and cavity mode spot sizes and smaller number of ions in a lower lasing level.

Fig. 5 shows the the emission cross section σ_e at the laser wavelength and the minimum pump intensity I_{min} required for achieving transparency at the laser wavelength [24]. This can be used as a figure of merit to classify different hosts. I_{min} can be calculated as following:

$$I_{min} = \frac{\sigma_a}{\sigma_e + \sigma_a} \frac{h\nu}{\sigma_{ap}\tau} \tag{14}$$

where σ_a is the absorption cross section at the laser wavelength, σ_{ap} is the absorption cross section at the pump wavelength.

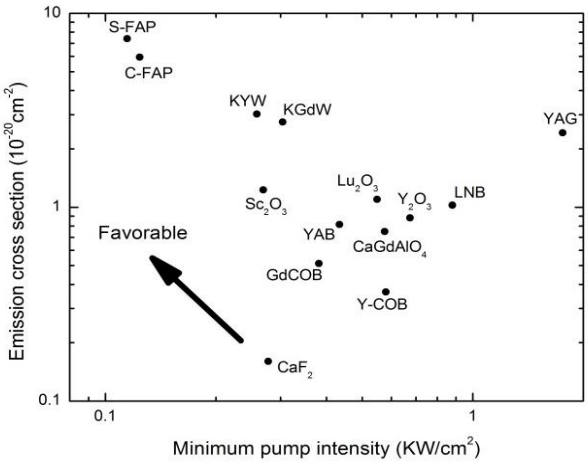

Figure 5: Figure-of merit for different Yb-doped crystals

Crystals of Yb:KYW and Yb:KGdW have one of the highest laser potentials while Yb:YAG and Yb:LNB crystals have the lowest [24].

3.6 Optical, physical and thermal properties

Yb:KYW is a highly anisotropic crystal with three optical axes denoted as N_p, N_m and N_g with refractive indices of n_p, n_m and n_g, respectively. Yb:KYW has high refractive indices of around 2 which is suitable for the fabrication of integrated optical devices [25]. Table 2 shows the measured values of the principal refractive indices of Yb:KYW published in various papers.

Table 2. Principal refractive indices for pure and doped KYW at different wavelengths

			Refractive index (n)		
Reference	Doping	λ	**E//N_p**	**E//N_m**	**E//N_g**
Loiko *et al.* [26]	-	436	2.0518	2.1008	2.1527
	-	633	1.9979	2.0396	2.0869
Kaminskii *et al.* [21]	-	633	1.9972	2.0392	2.0848
	-	1064	1.9688	2.0065	2.0507
Fillipov *et al.* [27]	-	632.8	1.99784	2.03971	2.08684
	(20 at.%)	632.8	2.00418	2.04488	2.09253
Fillipov *et al.* [28]	-	632.8	1.99784	2.03964	2.08684

The principal refractive indices satisfy the equation $n_p < n_m < n_g$ and decrease for longer wavelengths of light.

Having a high nonlinear refractive index, n_2, is essential for achieving ultrashort pulses using the Kerr-lens mode-locking technique. Determining exact values of n_2 is difficult and various literature state different values, but it is agreed that Yb:KYW has large values of nonlinear refractive index. The nonlinear index coefficient was reported to be $n_2 = 8.7 \times 10^{-16}$ cm^2/W at the wavelength of 1.08 μm [29]. However, this measurement was not performed for the light polarization parallel to any of the refractive axes. Vodchits *et al.* performed a Z-scan measurement of n_2 at 790 nm and 395 nm for the light polarization parallel to the N_p direction. Thilmann *et al.* also measured n_2 values for

the N_m and N_p polarizations at 819 nm using the Z-scan measurement technique. The results of these measurements are presented in Table 3.

Table 3. Nonlinear refractive indices of pure KYW and Yb-doped KYW at different wavelengths

			$n_2(\times 10^{-16} cm^2 W^{-1})$		
Reference	Doping	λ	**E//N$_p$**	**E//N$_m$**	**E//N$_g$**
Vodchits *et al.* [30]	-	395	36 ± 7	-	-
	-	790	21 ± 3	-	-
Thilmann *et al.* [31]	-	819	15	24	-
	(5 at.%)	819	15	19	-

Thermal conductivity, thermal expansion and thermo-optic coefficient (*dn/dT*) are the three major thermo-optic properties of a laser material which play an important role in power scaling of solid state lasers.

The thermal expansion coefficient is defined as the fractional change in the length per unit change in temperature. Yb:KYW is an anisotropic material; therefore, thermal expansion is different in different directions. Thermal expansion coefficients for pure and Yb-doped KYW crystal were studied widely and presented in Table 4. The largest expansion occurs along the N_g axis, while the N_p axis experiences the lowest thermal expansion.

Table 4. Comparison of thermal expansion measurements of pure KYW and Yb-doped KYW

		$\propto (\times 10^{-6} K^{-1})$		
Reference	Doping	**E//N$_p$**	**E//N$_m$**	**E//N$_g$**
Loiko *et al.* [26, 32]	-	2	10.8	17.4
Loiko *et al.* [33]	-	2	10.3	15.9
	(20 at.%)	2.9	10.7	15.2
Pujol *et al.* [34]	-	1.9	10.31	15.99
Aggarval *et al.* [35]		2.8	-	-

Thermo-optic coefficient, *dn/dT*, defines the temperature dependence of the refractive index in the material. Basically it represents the change in refractive index due to a

change in the temperature. Published values of thermo-optic coefficients, *dn/dT*, of pure and Yb-doped KYW are listed in Table 5 at various wavelengths.

Table 5. Thermo-optic coefficients *dn/dT* for pure and Yb-doped KYW

Reference	Doping	λ	dn/dT ($\times 10^{-6}K^{-1}$)		
			E//N$_p$	**E//N$_m$**	**E//N$_g$**
Loiko *et al.* [26]	-	633	-10.1	-7.3	-8.4
Loiko *et al.* [33]	-	1064	-14.6	-8.9	-12.4
	(20 at.%)	1064	-13.1	-7.6	-11.8
Fillipov *et al.* [27]	-	632.8	-7.98	6.73	-14.10
	(20 at.%)	632.8	-14.32	6.55	-14.30
Fillipov *et al.* [28]	-	632.8	-8	6.7	-14.1

According to [27, 28] dn_m/dT is positive while dn_p/dT and dn_g/dT are negative. The measurements were performed using the interferometric method and imply that n_p and n_g decrease, and n_m increases with an increase in temperature. However, the absolute values of thermo-optic coefficients increase with the wavelength and satisfy the relation $|dn_p/dT| > |dn_g/dT| > |dn_m/dT|$. Loiko *et al.* in [26] measured dn/dT using a minimum deviation method and found that thermo-optic coefficients are all negative in the spectral range 0.36-1.06 μm. This implies that principal refractive indices decrease with an increase in temperature. Loiko *et al.* stated that the change in the dimension of the material caused by anisotropic thermal expansion effect can have an influence on the measurements of thermo-optic coefficients.

Thermal conductivity (*K*) is defined as the ability of a material to conduct and transfer heat. Heat transfer rate is higher in materials with higher thermal conductivity; therefore, in high power lasers a material with high thermal conductivity is preferred. Yb-doped monoclinic double tungstates have a moderate thermal conductivity of around 3 $Wm^{-1}K^{-1}$ [21]. Exact values of the thermal conductivity of KYW crystal for different optical axes are not yet known. Thermal conductivity of undoped KYW was reported as 3.3 $Wm^{-1}K^{-1}$

[36]. Aggarval *et al.* measured the thermal conductivity of KYW along the N_p axis at different temperatures and found the value to be 2.7 $Wm^{-1}K^{-1}$ at 298 K [35]. The thermal conductivity increases as the crystal temperature decreases. Comparison of thermal conductivity of KYW, KLuW and KGdW crystals is presented in Table 6.

Table 6. Comparison of thermal conductivity between KYW, KGdW and KLuW

Reference		$K(\times 10^{-6}K^{-1})$		
		E//N$_p$	**E//N$_m$**	**E//N$_g$**
Biswal *et al.* [37]	**KGdW**	2.5	3	3.5
Silvestre *et al.* [38]	**KLuW**	2.36	3.41	3.59
Pujol *et al.* [35]	**KYW**	2.7	-	-

Elastic and photoelastic properties of KYW crystals were also studied and showed the suitability of this material for production of acousto-optic devices [39]. The fluorescence lifetime of Yb:KYW was measured to be about 0.3 ms [40].

3.7 Absorption and emission

Absorption and emission play an important role in laser characteristics. Ytterbium has a simple two level energy scheme. The Stark energy level diagram of Yb:KYW at the temperature of 77 K is shown in Fig. 6 along with some possible electronic transitions [13]. The quasi-three-level nature of Yb-doped crystals results in the thermal population of electrons in lower laser levels and causes reabsorption of a part of the emitted light. To overcome this issue, high pump intensity and a good matching between pump and cavity mode is required [41]. The highest absorption cross section in Yb:KYW is at 981 nm which corresponds to a transition from the ground level to the lowest energy level in the $^2F_{5/2}$ manifold.

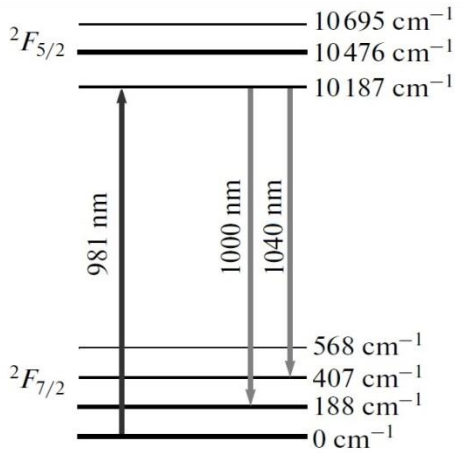

Figure 6: Stark-level energy in Yb:KYW at 77 K

Fig. 7 illustrates the absorption and emission cross sections of Yb:KYW with respect to the wavelength [42]. Yb:KYW has different absorption and emission cross sections along different axes, and the highest are along the N_m axis. The absorption peak along the N_m axis is found at 981.2 nm, which can be matched precisely with commercially available InGaAs laser diodes. The broad gain bandwidth and high emission cross section make Yb:KYW an ideal crystal for generation of ultrashort pulses.

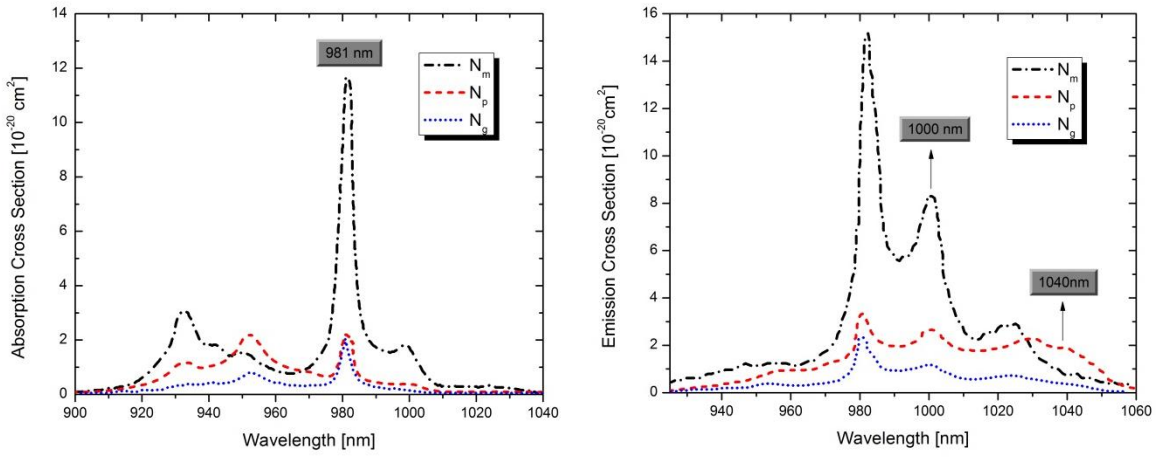

Figure 7: Absorption and emission cross section of Yb:KYW

The peak emission cross section is $\sigma_{em} = 3.10^{-20}$ cm^2 for light polarization parallel to the N_m optical axis at 1025 nm [13].

Some of the most important spectroscopic properties of Yb:KYW crystal are listed in Table 7, and Table 8 summarizes its physical characteristics.

Table 7. Spectroscopic properties of Yb:KYW and Yb:KGW

Parameter	**Yb:KYW**	**Yb:KGW**
Peak Absorption λ_{pump} (nm)	981.2	981
Absorption Linewidth (nm)	3.5	3.7
Peak Absorption Cross Section (cm^2)	1.33×10^{-19}	1.2×10^{-19}
Peak Emission Wavelength (nm)	1025	1023
Emission Linewidth (nm)	16	20
Peak Emission Cross Section (cm^2)	3×10^{-20}	2.8×10^{-20}

Table 8. Physical characteristics of KYW crystal [14]

Melting Point	~1080°C
Density	6.565 g cm–3
Specific Heat	~500 J kg–1 deg–1
Microhardness on the Mohs Scale	4–5
Optical Transparency (1 mm thick sample)	~0.34–5.5 μm

3.8 Effect of doping concentration

Doping can have significant effects on optical, physical and thermal properties of a laser crystal. As mentioned earlier, high doping concentrations of ytterbium can be achieved in KYW crystal due to the similar ionic radii of the dopant and crystalline host. In this section, the data of previous studies on doping effects on properties of Yb:KYW are presented.

Pure KYW and 20 at.% Yb:KYW were compared in [27] and it was shown that doping increases the principal refractive indices n_p, n_m and n_g of the pure crystal by 0.005–0.007. According to [33], doping of KYW crystal with Yb ions in the concentration of 20 at.% increases thermal expansion along N_p and N_m axes slightly and decreases the thermal expansion coefficient along the N_g axis. It was also observed that doping of KYW with Yb ions, increases the thermo-optic coefficients of the crystal. Naturally, doping also increases the absorption of pump wavelengths in a crystal. Demidovich *et al.* measured the fluorescence lifetime of Yb:KYW for different Yb concentrations and observed the rise in fluorescence lifetime with increase in doping concentration. The increase in lifetime can be explained by the increase in reabsorption losses and stronger radiation trapping with higher doping concentrations. From the results in [31] it can be observed that introducing Yb ions in KYW crystal can also substantially change the nonlinear index of refraction. From data in Table 3 it can be seen that anisotropy in the nonlinear refractive index was reduced in the KYW crystal doped with Yb ions. Generally, thermal conductivity of the material decreases with doping, but this effect has not been studied explicitly for the KYW crystal so far.

3.9 Pumping methods

Recent advances in diode lasers with wavelengths between 0.9 and 1.1 μm contributed to a high interest in diode pumped Yb^{3+} lasers. The Yb^{3+}ion is highly suited for laser diode pumping because of its single narrow absorption band while it is an impractical laser ion for flash-lamp pumping [43]. Reinberg *et al.* were the first to use a laser diode source to pump Yb ions in 1971 [44]. The existence of Yb^{3+}ion in KYW results in strong absorption at 981.2 nm. This wavelength is suitable for diode pumping with InGaAs laser diodes. InGaAs laser diodes are commercially available, cheap, compact and efficient. Laser diodes can be tuned to match the exact absorption bands of gain medium resulting in highly efficient pumping. Furthermore, laser diodes could have a long operating

lifetime in excess of 10,000 hours. These properties make InGaAs laser diodes highly suitable as the pump sources of Yb doped gain media.

3.10 Lasing history

The first continuous laser action of Yb:KYW at 1025 nm was demonstrated by Kuleshov *et al.* in 1996 with both Ti:sapphire and InGaAs laser diode as pumping sources [42]. Under Ti:sapphire pumping, slope efficiency of 78% was achieved, but under diode pumping slope efficiency of 10% was reported. The difference between slope efficiencies under diode and Ti:sapphire pumping was due to the use of a diode laser at 965 nm which does not match the high absorption peak of Yb:KYW at 981.2 nm. Also under diode pumping the crystal length used was 5 mm which resulted in poor overlap between the pump and cavity modes. A slope efficiency as high as 80% was achieved in continuous wave operation of Yb:KYW laser with crystal length of 0.7 mm [45]. Maximum CW output power of 72 W in multimode and 52 W in fundamental mode operation were obtained with thin-disk Yb:KYW laser [46]. High CW powers of 24W and 18.5 W was extracted in a diffraction limited beam using a dual-crystal resonator setup [47, 48].

KYW is highly suitable for waveguide geometry and fabrication of integrated optical devices due its high refractive indices. Yb:KYW waveguide was first demonstrated in 2006 by Romanyuk *et al.* with output power of 290 mW in the fundamental mode and the slope efficiency of above 80.4% [25].

Due to a broad gain bandwidth of Yb:KYW, an efficient tunable laser can be made around 1 μm. Wavelength tuning of 64 nm with maximum output power of 10.7 W and quantum defect of 0.6% was demonstrated in Yb:KYW thin-disk laser [4]. Similar experiments were performed to achieve tunable Yb:KYW using volume Bragg grating [49, 50, 51].

In 1997 Kuleshov *et al.* demonstrated the first pulsed Yb:KYW laser using a gain-switched Ti:sapphire laser with 30-ns pulse duration where a slope efficiency of 86% with respect to absorbed pump energy was achieved [13]. Excellent Yb:KYW pulsed lasers based on Q-switching and mode-locking techniques have been achieved over the past years.

In Yb doped tungstates the relatively long upper-state lifetimes is advantageous for Q-switching. Moreover, Yb:KYW is considered a reliable material for microchip lasers due to the high efficiency of laser operation provided by this crystal. Excellent Q-switched microchip lasers have been demonstrated. In 2002 Grabtchikov *et al.* demonstrated a Yb:KYW microchip laser which produced pulses with durations as short as 2 ns, a repetition rate of 49 KHz and maximum average power of 24 mW (peak power of 265 W) [19]. A similar Q-switched Yb:KYW microchip laser was demonstrated in 2007 which generated pulses with a duration of 34 ns and a repetition rate of 8 KHz with 70 mW of average output power (peak power of ≈ 300 W) [52]. In 2009 Bain *et al.* produced a Q-switched Yb:KYW planar waveguide laser with average output power of 30 mW, and pulses with duration of 170 ns at 722 kHz repetition rate [53]. A high power Q-switched laser based on dual-crystal resonator setup was demonstrated which generated 20 ns pulses with maximum average output power of 16 W at a repetition rate of 100 kHz [48].

Yb:KYW is also a great gain medium for producing ultrashort pulses of picosecond or femtosecond durations using mode-locking techniques. Relatively high thermal conductivity, high nonlinearity, low quantum defect, large emission cross sections and broad gain bandwidth are the properties that make Yb:KYW a suitable gain medium for ultrashort pulse generation. In 2001, for the first time, Liu *et al.* demonstrated Kerr-lens mode-locked Yb:KYW with pulses as short as 71 fs with 120 mW average output power

at a repetition rate of 110 MHz [54]. In 2002, the first SESAM mode-locked thin-disk Yb:KYW was demonstrated by Brunner *et al.* which produced 240 fs pulses at a repetition rate of 25 MHz and average output power of 22 W [55]. A repetition rate as high as 4.6 GHz [56] and slope efficiency of 69% [57] were reported in the mode-locking regime. Pulses as short as 66 fs were produced in SESAM mode-locked diffusion-bonded Yb:KYW/KYW [58]. Pulses with a peak power of 3 MW at 1 MHz repetition rate were generated from a cavity-dumped Yb:KYW laser. Using extra-cavity compression with a large-mode-area fiber and a prism sequence, pulses with duration of 21 fs and a peak power of 13 MW were generated [59]. Thin-disk Yb:KYW regenerative amplifiers were also demonstrated [60, 61].

Self-frequency conversion has been observed due to the high Raman gain coefficient of Yb:KYW [19]. Second harmonic generation was demonstrated with 138 mW at 500 nm [62] and 35 mW at 501.7 nm [63]. An optical frequency comb in the 1 μm spectral range was also demonstrated using Yb:KYW crystal [64].

Chapter 4

Experimental Characterization of Thermal Lensing

Before building a laser in the laboratory, a Z-cavity was designed and simulated using an ABCD matrix analysis. The cavity was designed to have a good overlap between the pump and the cavity modes to achieve efficient lasing. When designing the cavity, the effect of the thermal lensing was also considered.

4.1 Laser cavity design

The parameters used to achieve a cavity with desirable beam waists are shown in Table 9. These parameters are according to the lens equivalent waveguide of the Z-cavity shown in Fig. 3. The pump diode used in the experiment was coupled into a fiber with a core diameter of 110 μm. A collimating lens with focal length of 30 mm and a focusing lens with focal length of 100 mm were used to re-focus the pump beam into the crystal. The pump beam waist inside the crystal was therefore calculated to be 366 μm. The cavity should be designed such that the pump spot and the cavity mode sizes would match inside the crystal.

Table 9. Parameters used in equivalent lens waveguide of designed cavity

	Parameters							
	L_1	L_2	L_3	L_4	R_1	R_2	C_r	L_{Total}
Length (mm)	460	276	438	1055	500	750	2	2231
n	1	1	1	1	-	-	2	-

By substituting the values for L_1, L_2, L_3, L_4, R_1, R_2 in their corresponding transfer matrices and multiplying them we found the M_T to be:

$$M_T = \begin{bmatrix} -0.155 & 90.903 \\ -0.011 & -0.269 \end{bmatrix} \tag{15}$$

Therefore, $A = -0.155, B = 90.903, C = -0.011, and\ D = -0.269$

In order to calculate the mode size inside the gain medium Eq. 10 can be used where $\lambda = 1041\ nm$:

$$w^2 = \frac{\lambda|B|/\pi}{\sqrt{1-(D+A)^2/4}} = \frac{1041 * 10^{-6} * 90.903/3.1416}{\sqrt{1-(-0.269 \pm 0.155)^2/4}} = 0.0308\ mm^2$$

$$w = \sqrt{0.0308} mm = 175.5 \mu m$$

The smallest mode size occurs at distance $L = 737\ mm$ which corresponds to the position of the crystal within the cavity. The mode size at this position is $175.5\ \mu m$ as calculated earlier. Variation of the mode size within the cavity is shown in Fig. 8.

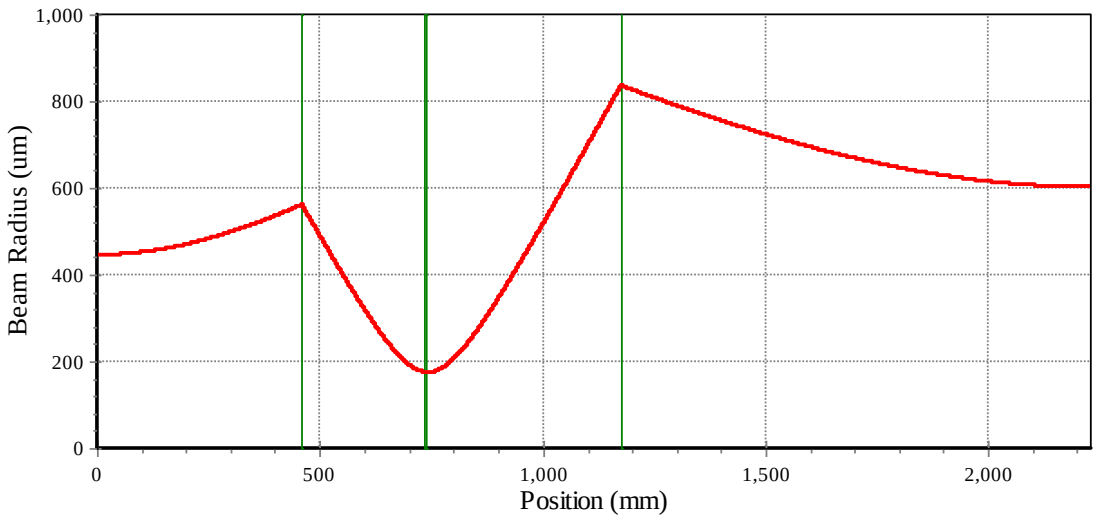

Figure 8: Mode size inside the cavity

Thermal lens can be modeled as a thin lens inside the crystal. The strength of the thermally induced lens can have a significant effect on stability of the cavity. The

stability of cavity can be evaluated against the focal length of the induced thermal lens by placing a lens element inside the gain medium and varying its focal length. Fig. 9 shows the stability diagram of the designed cavity with respect to the focal length of the induced thermal lens. Stability condition in Eq. 12 defines the regions where the cavity is stable.

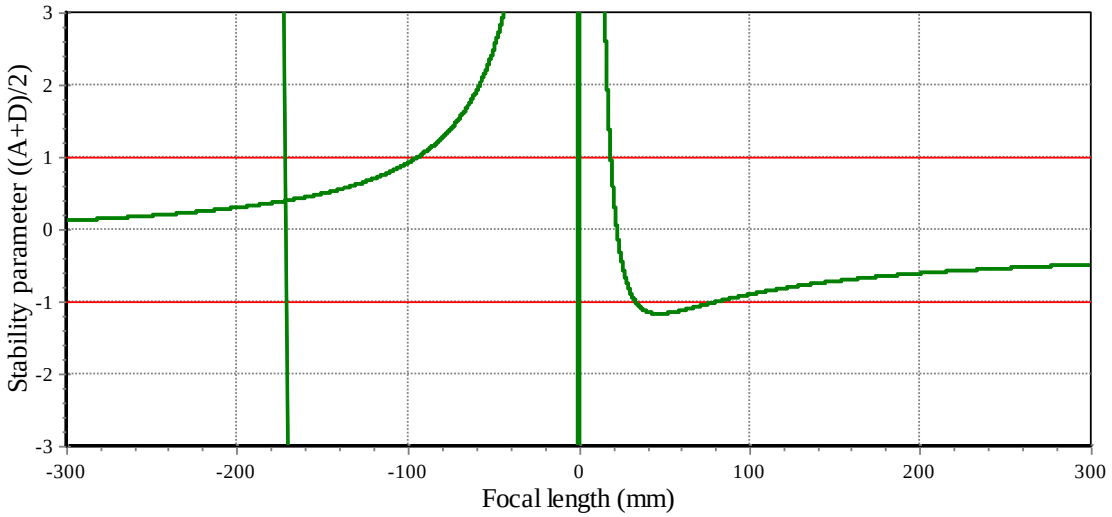

Figure 9: Stability diagram with respect to changes in focal length of the induced lens

The variation of the beam radius at output coupler (M4) with respect to the changes in the focal length of the induced thermal lens is shown in Fig. 10.

ABCD modeling shows that strong positive thermal lensing results in the increase of output mode diameter at the output coupler, and strong negative thermal lensing causes decrease in output mode diameter at the output coupler. As can be seen from Fig. 10, a strong positive or negative thermal lens ($< 100\ mm$) can result in an unstable cavity.

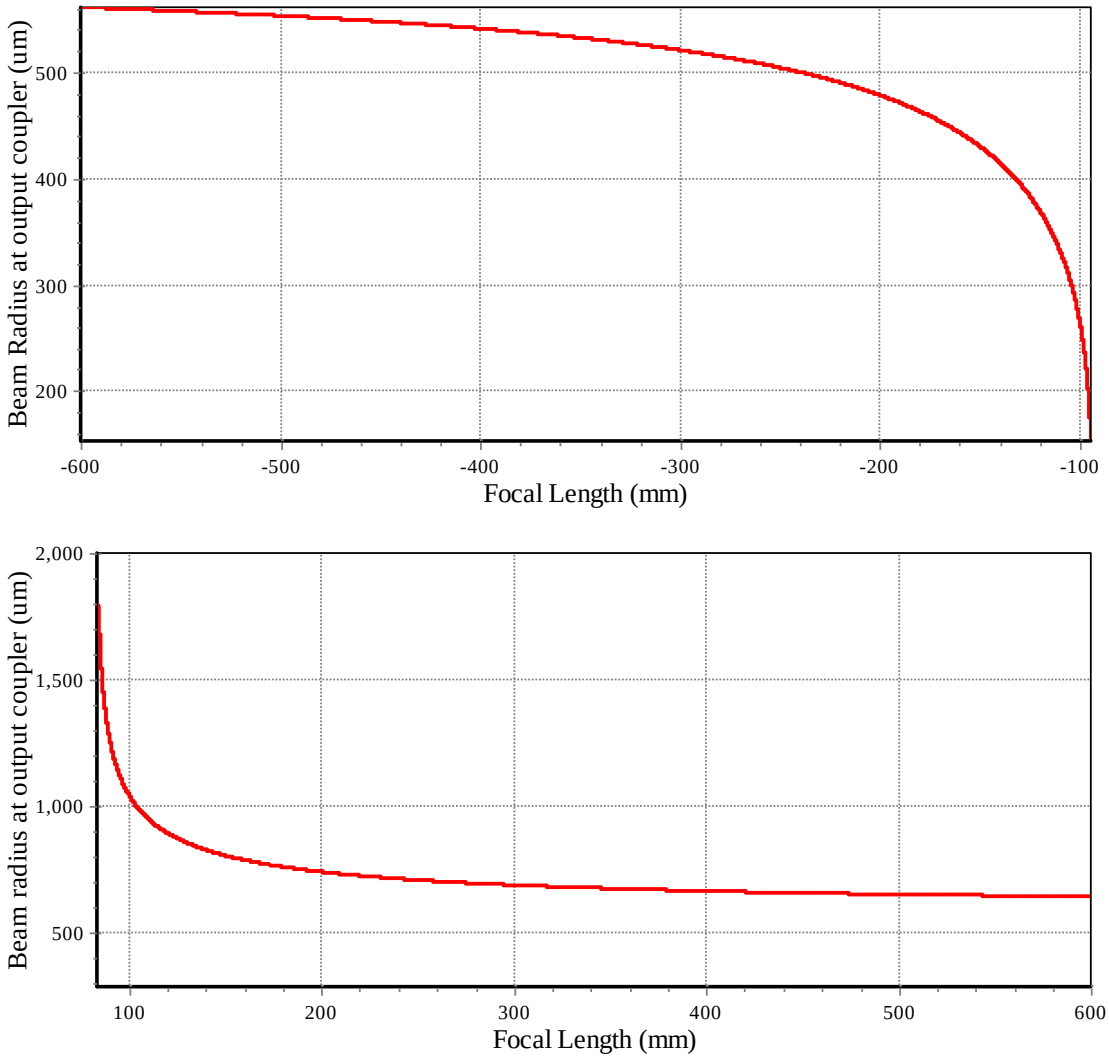

Figure 10: Beam radius at output coupler with respect to the focal length of the induced lens

4.2 Experimental setup

This section starts with a description of the laser diode used for pumping Yb:KYW laser crystal. Procedures used to construct the continuous wave Yb:KYW laser are explained, and finally the measurements about the laser performance are presented.

4.2.1 Pump laser

The pump laser was a fiber-coupled 25 W laser diode operating around 980 nm (PLD-30-C-980, IPG Photonics Corp). The fiber had a core diameter of 110 μm and a numerical aperture of 0.12. The light emitted by a laser diode was linearly polarized, but the polarization was not maintained through the fiber and the output beam from the fiber is not polarized. The output power from the diode laser was measured at different drive currents as shown in Fig. 11. The threshold current was about 0.6 A, and the maximum output power obtained was about 25 W at 11.7 A of drive current.

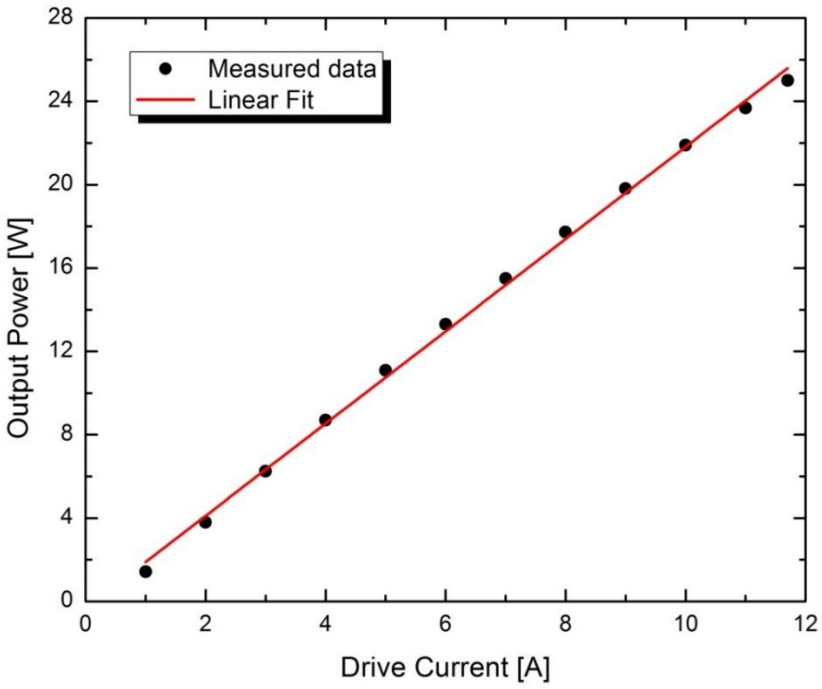

Figure 11: Output power from the diode laser versus drive current

An optical spectrum analyzer was used to analyze the spectrum of the diode laser. As shown in Fig. 12, the wavelength of the laser diode is tunable by changing the temperature. The wavelength of the laser diode shifts towards longer wavelength with increasing drive current. The pump source had a typical spectral width of about 4 nm. In order to increase the absorption of pump in the Yb:KYW, the temperature of the laser diode should be optimized such that the wavelength matches the absorption peak ($\Delta\lambda\sim$

3.5 nm) of the crystal at 981.2 nm. The beam quality, M^2 factor, of the laser diode was calculated to be ~20.

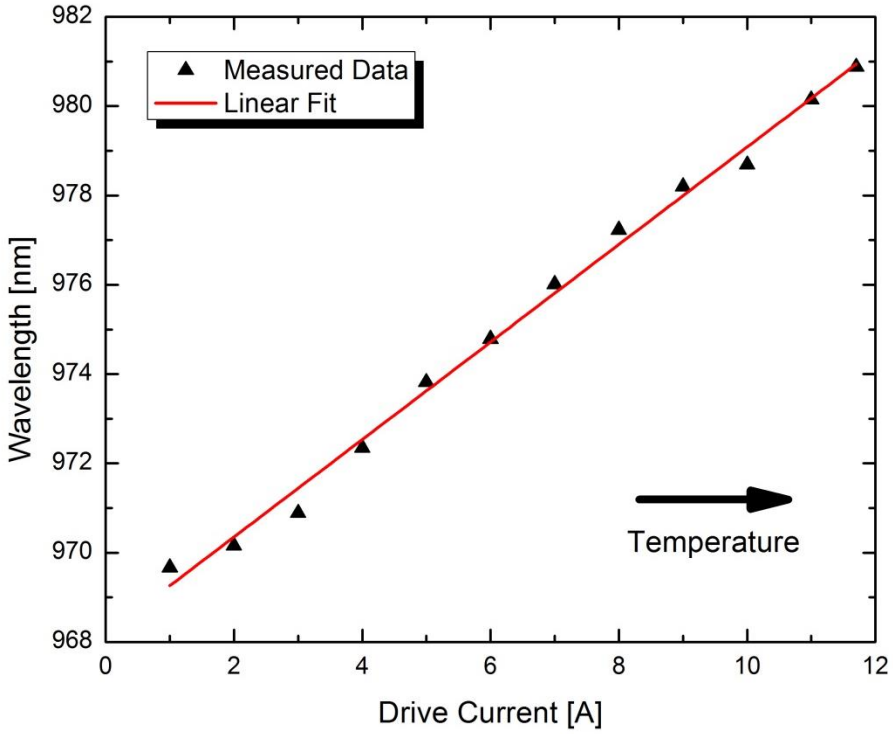

Figure 12: Laser diode wavelength vs. drive current

4.2.2 CW laser

The schematic diagram of experimental setup of a diode pumped continuous wave Yb:KYW laser is presented in Fig. 13. A 2 mm long (N_g-cut) 5 at. % Yb^{+3}-doped KYW crystal was used as the active medium. The output from the fiber-coupled laser diode was first collimated with a f = 30 mm collimator lens and, subsequently, focused onto the laser crystal by a f = 100 mm focusing lens through a dichroic mirror M1. The pump light incident on the laser crystal was unpolarized.

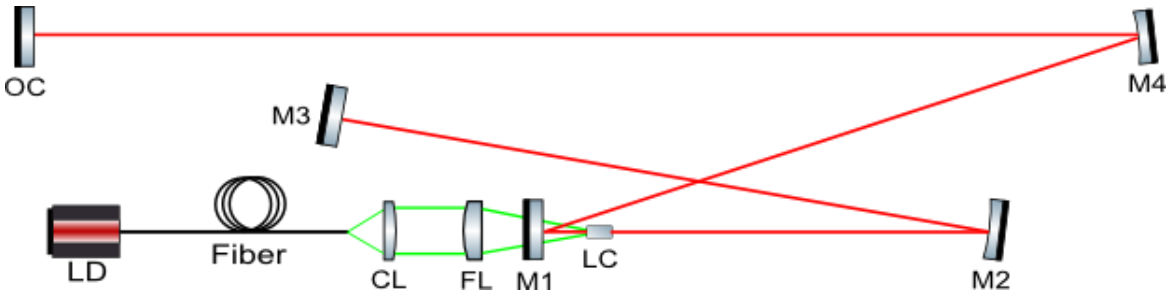

Figure 13: Schematic diagram of a CW Yb:KYW laser: (LC) Yb:KYW laser crystal; (CL) *f*=30 mm collimating lens; (FL) *f*=100 mm focusing lens; (M1) flat dichroic mirror (M2) curved mirrors with ROC =500 mm; (M4) curved mirrors with ROC =750 mm; (M3) HR mirror; (OC) output coupler (8% transmission); (L) *f*=150 mm lens

According to simulations, the cavity beam waist radius inside the crystal was about 175 μm. The 1:3.3 imaging system used focused the pump beam to a spot size of about 180 μm, which is very close to the cavity mode. Indium foil was used to wrap the laser crystal to improve the thermal conduction between the laser crystal and the aluminum heat sink. The top and the bottom surfaces of the crystal were in contact with the aluminum heat sink and cooled by water at 16 ˚C at a flow rate of 0.7 liters/minute. The optical surfaces of the crystal were antireflection coated for both the pump (λ = 975-985 nm) and the output (λ = 1010-1070 nm) wavelengths. The resonator consisted of an HR flat mirror M_3 and spherical mirrors M_2 (radius r = 500 mm) and M_3 (radius r = 750 mm). The transmittance of the output coupler (OC) at the laser wavelength was T = 8%. A calibrated power meter was used to monitor the average output power.

4.2.3 Discussion and results

Incident pump power applied was limited to 20 W to avoid any damage to the crystal. With an 8% output coupler, a threshold of 7.5 W and a slope efficiency of 56% were measured with respect to the absorbed pump power as shown in Fig. 14. With respect to the incident pump power, the laser threshold was at 12.9 W with slope efficiency of 51%.

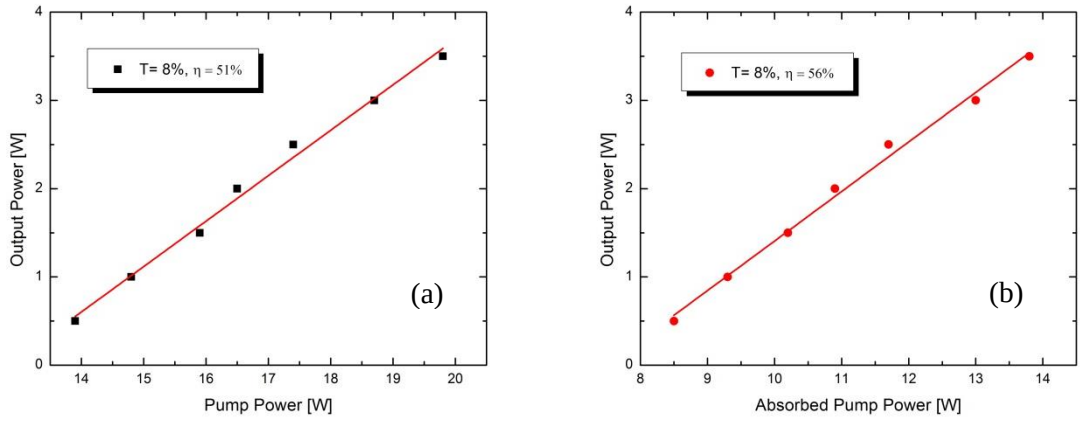

Figure 14: Output power versus (a) incident pump power and (b) absorbed pump power

Absorption in the crystal under nonlasing condition is about 61% for incident pump power of 13.9 W and corresponding output power of 0.5 W. The absorption in the crystal increases to 70% with incident pump power of 19.8 W which corresponds to a maximum output power of 3.5 W. It should be noted that absorbed pump power is smaller under nonlasing condition because of the saturation of absorption. In contrast, absorbed pump power is larger under lasing condition, because lasing brings the excited population back to a lower lasing level. It can be seen from Fig. 15 that absorption increases linearly as incident pump power increases. This increase in absorption can be explained by a wavelength shift of the laser diode (see section 4.2.1 in Chapter 4).

The maximum continuous wave output power reached was 3.5 W at the fundamental TEM_{00} mode (the M^2 factor was lower than 1.2 throughout the experiment).

The double-pass loss in the cavity can be estimated by the slope-efficiency data by the relation [13]:

$$\eta = \eta_0 \frac{T}{T + L_{int}} \tag{16}$$

Where T is the output coupling and η_0 is the intrinsic efficiency and L_{int} is the double-pass loss. The intrinsic efficiency can be determined by the quantum defect between the pump and laser wavelengths (980 nm and 1041 nm, respectively) in the absence of excited-state absorption, $\lambda_p/\lambda_{se} = 0.941$. The double-pass loss can be calculated to be 6.8%. The threshold pump power can be calculated from Eq. 13 where $\sigma_{aL} = 0.045 \times 10^{-20}$ and double-pass reabsorption losses can be calculated to be 2.5%. The emission lifetime of Yb:KYW is estimated to be 0.35 ms [40]. By substituting $\lambda = 980$ nm, ω_s and ω_p =175.5 μm and $\sigma_{em} = 0.59 \times 10^{-20}$at λ = 1041 nm we can calculate the threshold pump power $P_{th} = 13.5$ W which is close to our measured value of 12.9 W.

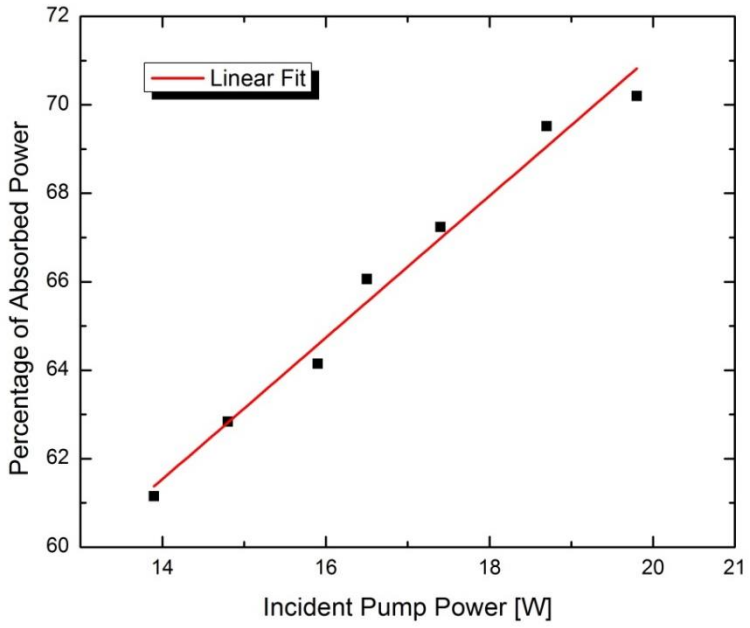

Figure 15: Percentage of absorbed pump power versus incident pump power

4.3 Measurement of thermal lensing

The goal of this experiment was to measure the focal length of the induced thermal lens in Yb:KYW under end pumping from a fiber coupled laser diode. In this section the method used to measure the thermal lensing is explained and the results are presented and analyzed.

4.3.1 Measurement method

Thermal lens depends directly on the absorbed pump power, and affects the beam quality depending on its strength. The M^2 ("M squared") is a measure of the beam quality of a laser beam and is affected by thermal lensing; therefore, it has to be measured for the different values of laser output power.

In order to measure the M^2 factor a lens was placed at a fixed distance from the output coupler, and a CCD beam profiler was used to measure the spot sizes of the focused beam as shown in Fig. 16.

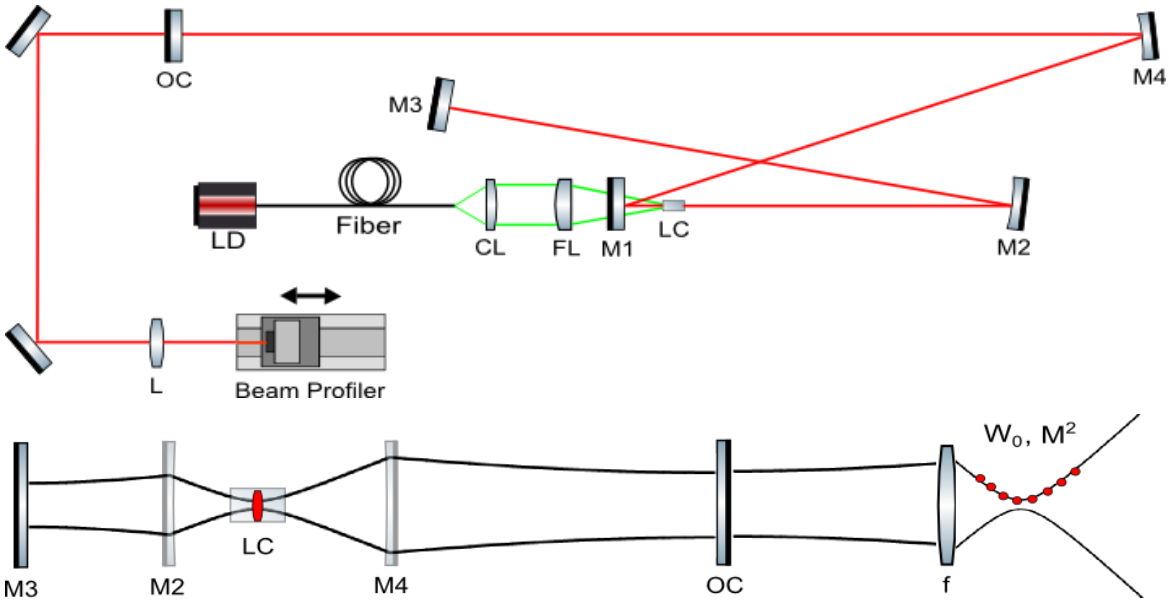

Figure 16: Beam radius variation and beam quality measurement

The M^2 factor and the beam waist, W_0, of the laser beam were then determined by fitting the measured spot sizes to the Gaussian propagation equation given by [65]:

$$W(z) = W_0 \left[1 + \left(\frac{M^2 \lambda_0 z}{n\pi W_0^2}\right)^2\right]^{1/2} \tag{17}$$

where λ_0 is the wavelength of the light and z is the position along the propagation direction of the beam. The thermal lens can be modeled as a thin lens inside the crystal with different focal lengths for different laser output powers. A laser cavity with a variable lens can be simulated using the ABCD matrix roundtrip model to find the focal length at which the beam waist from the model matches the beam waist obtained from the experimental measurement. It is important to note that the M^2 factor used in the ABCD modeling must have the same value that was measured experimentally at different output power levels. In this way the simulated laser cavity will be analogous to the experimental laser cavity, and the thermal lensing effect can be studied very accurately. An ABCD matrix roundtrip modeling with variable lens and beam propagation outside of the cavity was performed with commercial LASCAD [66] software.

4.3.2 Measurement results

The beam quality of a laser was first measured for different output powers. The beam was focused by a lens with f = 150 mm and the beam radii were measured for several points along the propagation direction using the beam profiler. The beam radii at each position were measured ten times and averaged to reduce the measurement errors. The beam waist W_0 and the beam quality factor M^2 were found by fitting Eq. 17 to the measured data. As an example, the data and fitting curves for output powers of 1 W and 3 W are shown in Fig. 17. The M_x^2 represents beam quality in horizontal plane and the M_y^2 represents the beam quality in vertical plane.

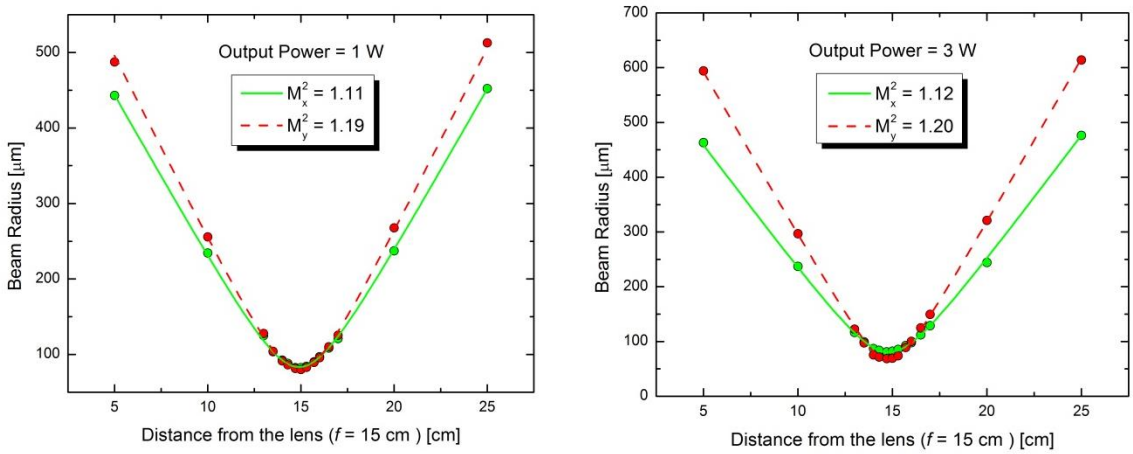

Figure 17: Laser output beam quality M^2 at 1 W and 3 W output power

The output power with respect to the incident pump power, along with corresponding M^2 values, are shown in Fig. 18. Near diffraction limited beam quality (M^2<1.2) was obtained throughout the experiment.

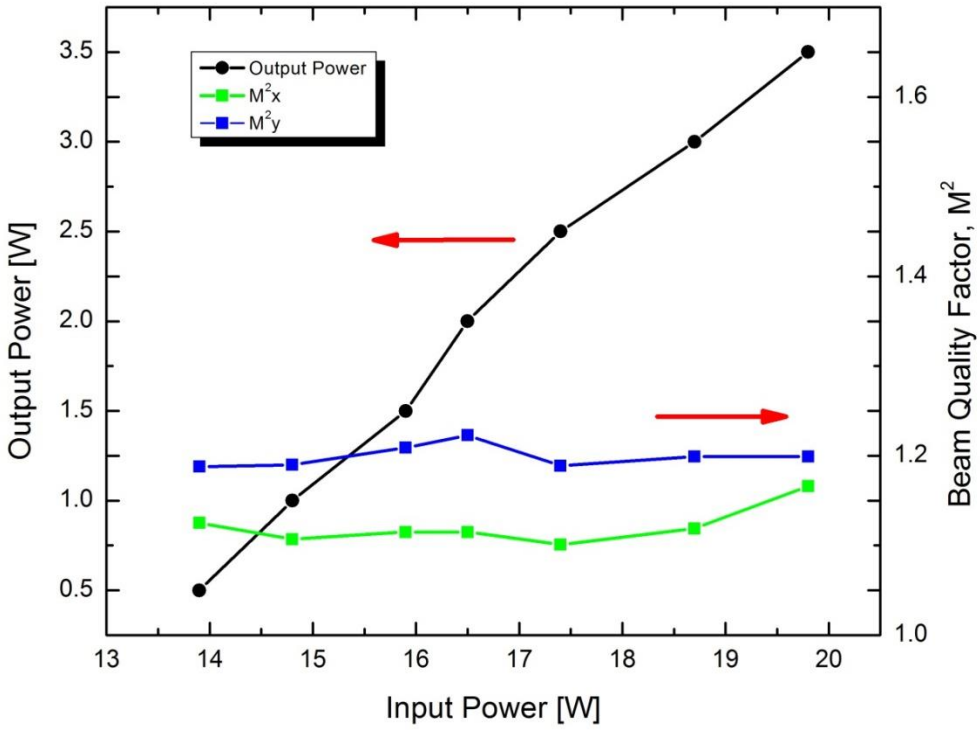

Figure 18: Output power and M^2 values (horizontal and vertical)

In order to measure the thermal lens, the beam waist of the laser beam was measured using the beam profiler. The beam waists at different output powers can then be compared to the simulated results of the resonator using LASCAD software. Fig. 19 shows the output beam waist radius at the focal plane of the lens (f = 150 mm) with respect to the absorbed pump power.

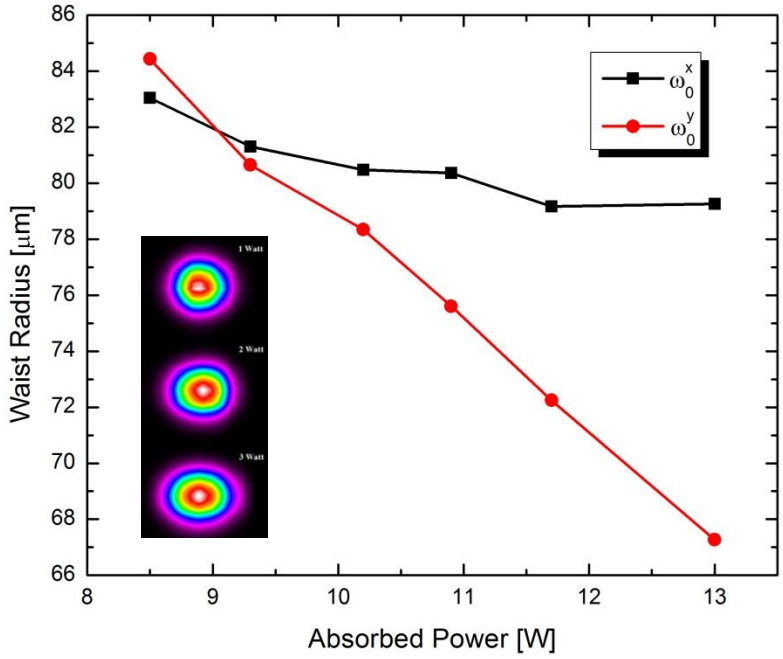

Figure 19: Waist radius versus the absorbed power after the lens (f = 150 mm)

Our previous ABCD modeling of the cavity in Section 4.1 showed that a positive thermal lens results in an increase of the beam diameter at the output coupler, while a negative thermal lens results in a decrease. According to our experiments the beam output diameter after the output coupler increased with increasing of the incident pump power; therefore, the thermal lens in the constructed diode pumped N_g-cut Yb:KYW crystal is positive in horizontal and vertical directions. The beam intensity profile was also measured by a beam profiler at approximately 42 cm distance from the output coupler.

As can be seen from Fig. 19 the output beam is very close to a Gaussian beam even at the high output powers, although the output beam becomes slightly elliptical. According to our ABCD modeling and measurements, the output beam dimension increases as thermal lens gets stronger. The thermal lens is stronger in the vertical direction which leads to a higher divergence in the vertical direction and results in slight ellipticity of the output beam.

Variation of focusing power of the thermally induced lens is estimated by using the ABCD matrix analysis and is shown in Fig. 20. It can be seen that the thermal lens is much stronger in the N_p direction compared to the N_m direction. This can be explained by cooling geometry, lower thermal conductivity and higher thermo-optic coefficient dn/dT of the Yb:KYW in the N_p direction.

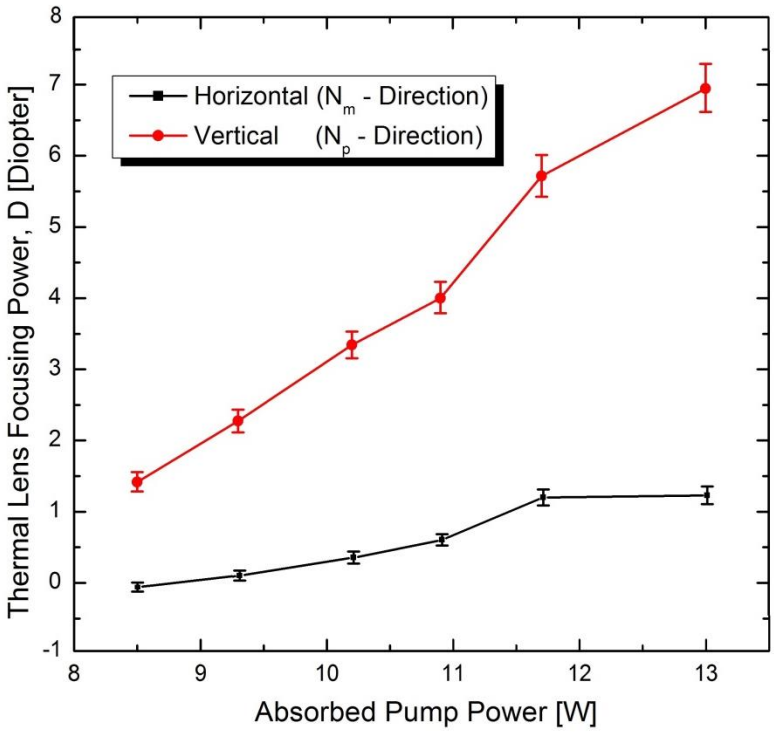

Figure 20: Thermal lens focusing power for vertical and horizontal directions

Thermal lens focusing power for bulk Yb-doped laser crystals under diode pumping is defined as [5]:

$$D = \frac{P_{abs}\eta_h\chi}{2\pi\omega_p^2 K_c} \tag{18}$$

where D is the thermal lens focusing power in diopters, P_{abs} is the absorbed pump power, η_h is the fraction of the absorbed pump power dissipated as heat, and χ is the generalized thermo-optic coefficient which includes thermo-optic, photoelastic and bulging effect. According to this equation the relationship between the absorbed pump power and the thermal lens focusing power is linear. The estimated error in the absorbed pump power measurement was 5%. This causes an error in the measurement of the thermal lens focusing power at specific pump power level. Another source of error lies in the beam width measurement. Although the beam radii at each position were measured ten times and averaged, there is still an uncertainty of about ±5 μm in the measurements. This uncertainty also results in uncertainty in the calculated beam waist, W_0, at each power level, and consequently affects the thermal lens measurement. The error bars shown in Fig. 20 correspond to the calculated uncertainty due to the measurements of the absorbed pump power and the beam width.

The results in Fig. 20 show that the thermal lens focusing power differs by up to 7 times in the horizontal and vertical directions at the highest pump power. The thermal lens is astigmatic (stronger in vertical direction). The degree of astigmatism is weaker for lower pump powers and strong astigmatism can be observed for higher pump powers. This behavior can be explained by the anisotropic thermal properties of Yb:KYW for different directions and non-symmetrical cooling geometry of the Yb:KYW slab.

Thermal lens sensitivity factors, *M*, can be calculated as:

$$M = \frac{dD}{dP_{abs}} \tag{19}$$

Thermal lens sensitivity factors were calculated to be 1.26 m^{-1}/W and 0.32 m^{-1}/W for the N_p and N_m directions, respectively.

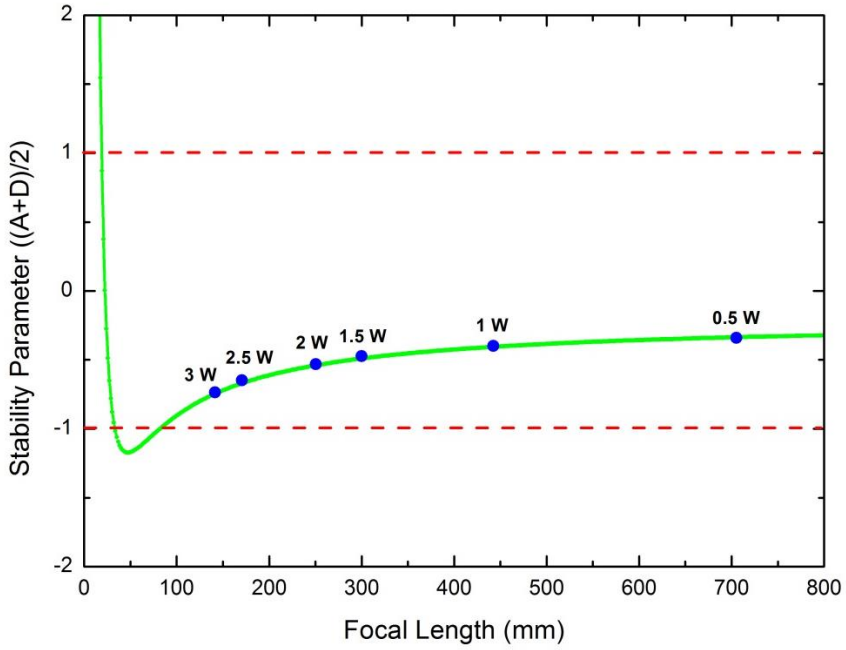

Figure 21: Cavity stability at different output powers

It can be seen from the experimental results that the Yb:KYW has serious thermal lensing effects. At maximum output power, the cavity is on the verge of stability due to the strong thermal lensing. It can be seen in Fig. 21 that at 3 W output power, focal length of the measured thermal lens is 144 mm. According to our cavity design, the cavity becomes unstable if the focal lens of thermal lens gets shorter than 83 mm. A further increase in output power will cause the cavity to become unstable.

A number of factors affect the thermal lensing such as crystal geometry, crystal orientation, doping concentration, pump wavelength, pump geometry, cavity design and

cooling geometry. All these factors can be optimized in order to reduce the thermal lensing. For example the pump wavelength can be chosen such that absorption coefficients of the N_p and N_m polarizations are equal. As can be seen from Fig. 7, at 947 nm the absorption coefficients of these two polarizations are equal. This pump design can make the heat distribution more uniform along the crystal length which leads to a reduction of thermal lensing and improving the beam quality while maintaining the output power. More efficient heat removal by liquid nitrogen or liquid helium can also result in reduction of thermal lensing effect due to the increase in thermal conductivity of the KYW as can be seen from Fig. 22 [35].

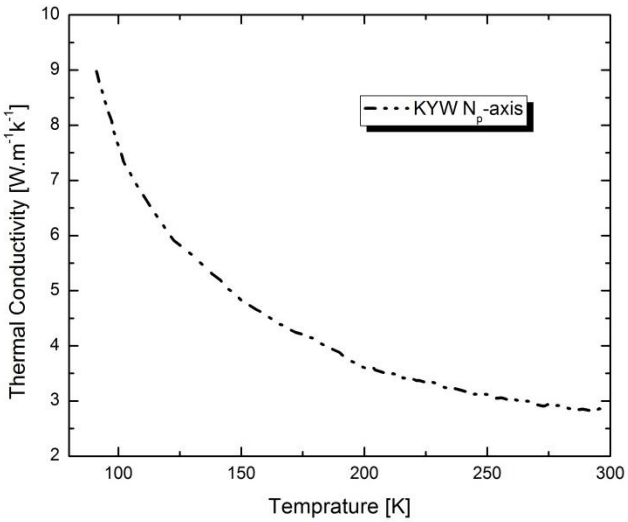

Figure 22: Thermal conductivity versus temperature for the undoped KYW

Chapter 5

FEA Simulation

5.1 Simulation of thermal lensing

Finite element analysis (FEA) method can be used to calculate the temperature and stress fields in the laser crystal. FEA method allows us to analyze the thermal lensing effect thoroughly and obtain the focal length of the induced thermal lens inside the crystal. In this chapter we discuss the use of the commercial LASCAD software to simulate the temperature distribution, deformation, and stress in our laser crystal. FEA method allows for the solving of the complex heat diffusion differential equation. Results of thermal analysis are used for the simulation of thermal lensing effects for our particular pump configuration and cooling system. The parameters of Yb:KYW used in our FEA are listed in Table 10.

Table 10 Parameters of Yb:KYW used in finite element analysis

	Priciple refractive axes			
	$E//N_p$	**$E//N_m$**	**$E//N_g$**	Reference
Thermal conductivity ($Wm^{-1}K^{-1}$)	2.36	3.41	3.59	[38]
Thermal expansion ($10^{-6}K^{-1}$)	2.9	10.7	15.2	[33]
Young's modules (10^9 Pa)	152.5	112.4	94.2	[67]
Poisson's ratio		~ 3		[67]
Refractive index	1.9688	2.0065	2.0764	[21]
dn/dT ($10^{-6}K^{-1}$)	-2.8	-8.9 [68]	-12.4 [68]	-

Unpolarized pump power of 20 W with 175 μm waist radius is incident on the Yb:KYW crystal. The pump beam has a circular shape and the intensity profile of the pump beam is assumed to be top-hat which is flat over most of the pumped region. The crystal is 2 mm long along z-axis, 5 mm wide along x-axis and 1.2 mm thick along y-axis as shown in

Fig. 23. Both the top and the bottom (x-z) surfaces of the crystal were cooled by water at 16 ˚C. The flow rate of water was set to 0.7 liters/minute.

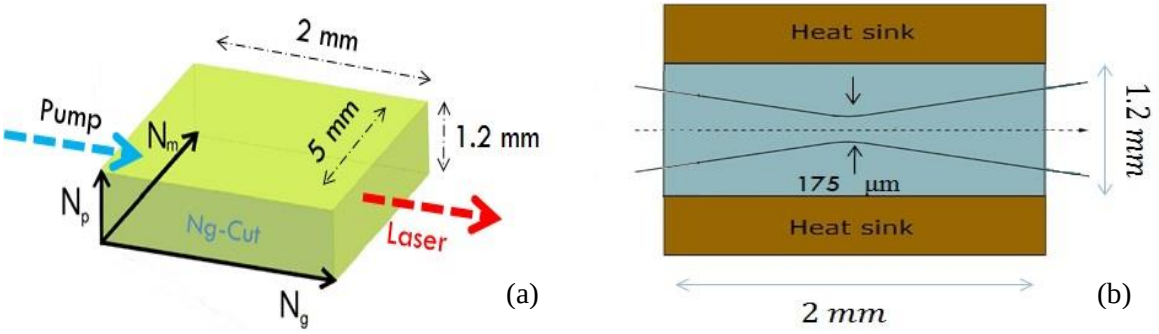

Figure 23 : (a) Crystal geometry (b) pump and cooling geometry

FEA was performed to calculate the temperature distribution in Yb:KYW crystal pumped by a fiber-coupled laser diode. The mesh size was chosen to be 50 µm in x, y and z directions with the estimated 97,750 elements. A smaller mesh size of 30 µm will increase the number of elements to 441,237 elements; however, the computation time will increase by more than 4 times. The difference between the calculated thermal lens focusing power between these two mesh sizes was less than 1%. The 50 µm mesh size was chosen for FEA analysis such that to achieve the highest accuracy with the lowest computation time. Fig. 24 shows the temperature distribution in the N_g-cut Yb:KYW crystal.

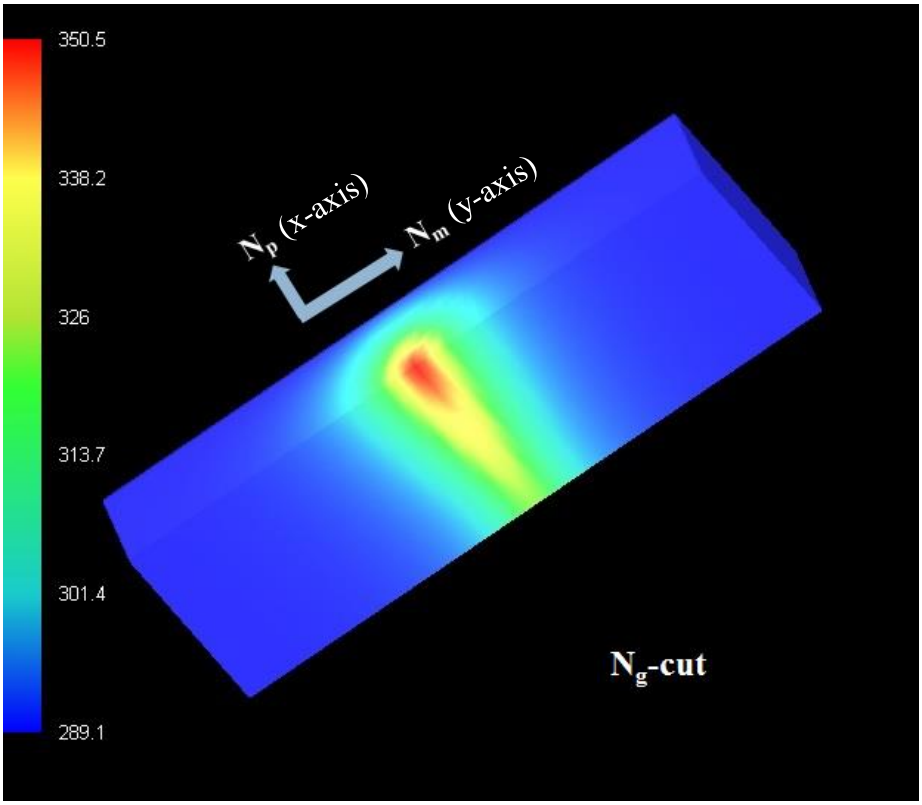

Figure 24: 3-D temperature cut in N_g-cut Yb:KYW

According to the FEA simulation at an incident power of 18.7 W corresponding to an output power of 3 W, the temperature inside the crystal reaches up to 75 C˚. It can be seen from Fig. 24 that the heat is mainly accumulated at the center of the pump spot and near the incident surface of the crystal where most of the power is absorbed.

The 2-D temperature distributions along the N_m-axis and N_p-axis at the front surface of the crystal and the parabolic fit of the temperature distribution and deformation are shown in Fig 25.

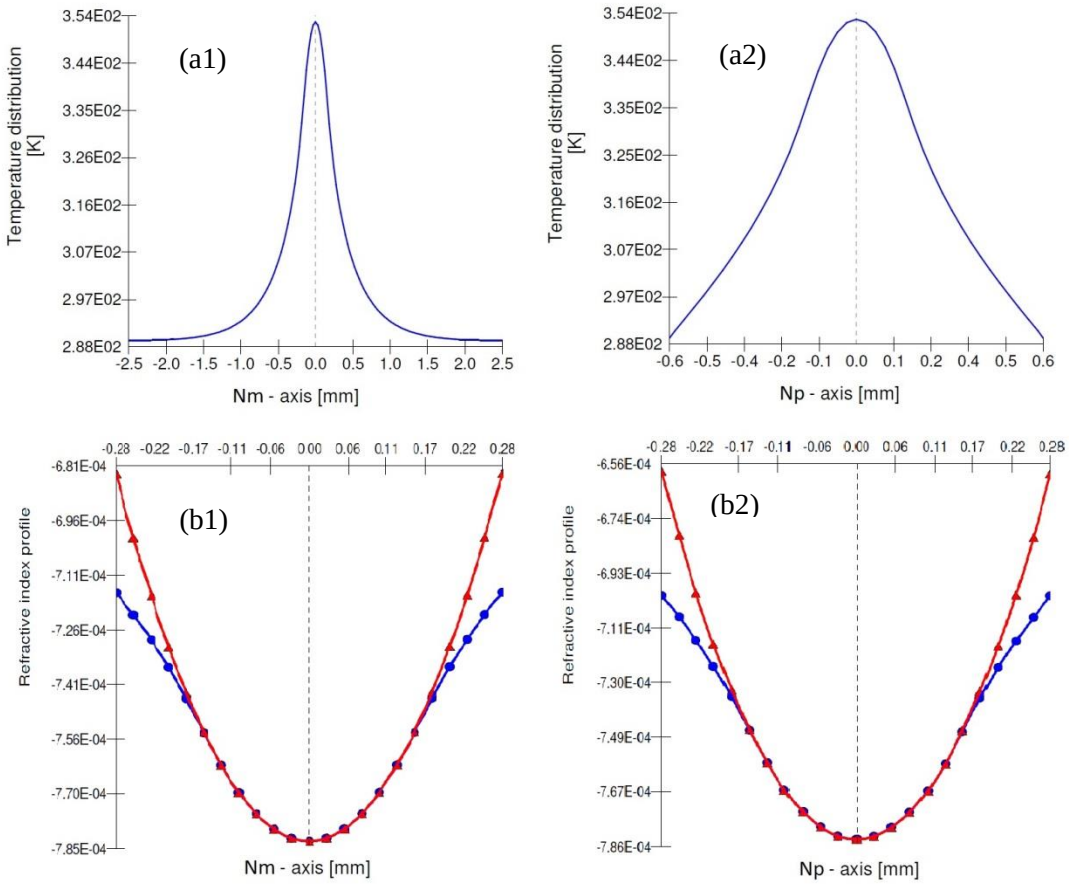

Figure 25: 2-D temperature distribution along the N_m-axis (a1) and N_p-axis (a2) at the front surface of the crystal. (b1) and (b2) are the parabolic fits of the temperature distributions and deformations along the N_m-axis and Np-axis, respectively.

LASCAD computes the refractive index distribution corresponding to the temperature distribution inside the crystal as shown in Fig. 25, and calculates the effective focal length of the induced thermal lens. The red curve in Fig. 25 (b) shows the parabolic fit of the refractive index profile in the pumped region of the crystal. The focal length was calculated to be 814 mm in the N_m direction and 141 mm in the N_p direction for the absorbed pump power of 13W. The same fitting procedure was performed for the different pump power levels and the obtained thermal lens focusing power is shown in Fig. 26 next to the experimental results.

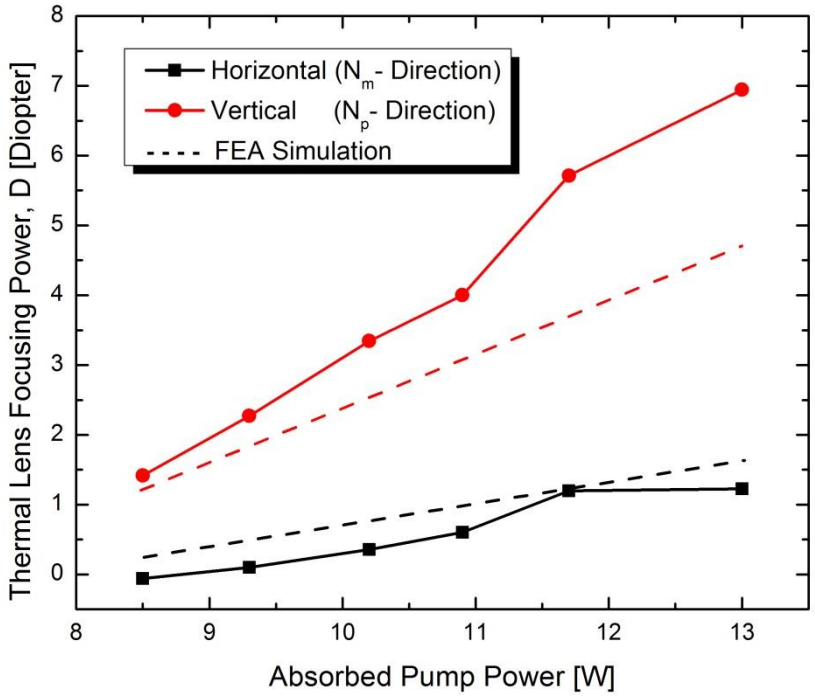

Figure 26: Comparison of thermal lensing between experiment and simulation

It can be observed that by using the parameters listed in Table 10, the FEA model provides a good estimation of the thermal lensing effect and results in the best matching between the simulation and experimental data.

In order to find the best fit, the $dn_p/d\mathrm{T}$ was varied and the corresponding R-squared, R^2, was measured. R-squared can be used to measure the goodness of the fit. As the fit gets closer to the data points, the R^2 will get closer to the value of 1. The values of R^2 for both the horizontal and the vertical directions were calculated to be 0.63 and 0.55 respectively. A smaller negative value than $-2.8 \times 10^{-6} K^{-1}$ will result in a slightly better fit for the vertical direction, but in worse fit for the horizontal direction. A larger negative value will result in a better fit for the horizontal direction, but in worse fit for the vertical direction. We found $dn_p/d\mathrm{T} = -2.8 \times 10^{-6} K^{-1}$ to be the best value to maximize the R^2 for both horizontal and vertical directions.

As was shown in Table 5 in chapter 2, there are discrepancies between the reported values of the thermo-optic coefficient for the Yb:KYW crystal. There is still a need for more accurate measurements and in-depth studies of this important parameter in Yb:KYW crystal. The difference between the experimental results and simulation results can further be justified, because LASCAD software does not take into account the photoelastic effect in thermal lensing calculations. The thermo-optic and bulging effect seem to be the most significant factors in thermal lensing [5], but for more accurate simulation the photoelastic effect should be also considered.

The results of the experimental measurements and FEA analysis show that the thermal lensing in the N_p-cut Yb:KYW is determined mainly by the thermal expansion and therefore by the face bulging. It can be concluded from the results that the face bulging is more dominant than the thermo-optical effect which results in an effective net positive thermal lens in our case.

Chapter 6

Final Remarks

6.1 Conclusion and future work

A diode-pumped Yb:KYW laser was successfully built in the laboratory. The laser was operating at the wavelength of 1.04 μm. It was designed to have a good overlap between the pump and cavity modes to achieve efficient lasing. A threshold of 7.5 W and a slope efficiency of 56% were measured with respect to the absorbed pump power. The maximum output power achieved was 3.5 W corresponding to the incident pump power of 19.8 W. Nearly diffraction limited output beam ($M^2 < 1.2$) was achieved in both horizontal and vertical directions for all output power levels. Detailed studies of the thermal lensing in Yb:KYW lasers were performed for the first time. The focal lengths of the induced thermal lenses were obtained from the laser output beam size measurements at various incident pump power levels and ABCD matrix analysis. At maximum output power the focal length of the induced thermal lens was found to be 814 mm for the N_m direction (horizontal) and 144 mm for the N_p direction (vertical). Thermal lens sensitivity factors were determined to be 1.26 m^{-1}/W and 0.32 m^{-1}/W for the N_p and N_m directions, respectively. This highly astigmatic thermal lensing can be explained by a strong anisotropy of the thermo-optical properties of the crystal and its cooling geometry.

In the second part of the work, the finite element analysis (FEA) method was used to calculate the temperature and stress fields in the laser crystal. FEA method allows us to analyze the thermal lensing effect thoroughly and obtain the focal length of the induced thermal lens inside the crystal. The results of simulations showed good agreement with the experimental data.

In future work, detailed studies of the thermo-optic parameters of Yb:KYW such as thermal conductivity and thermo-optic coefficient (*dn/dT*) for different doping levels should be considered. Furthermore, a detailed investigation of athermal direction in Yb:KYW is necessary. In athermal direction of propagation, stress and temprature dependent refractive indices compensate each other, and the thermal lensing effect will be reduced. In addition, more studies on the effect of crystal geometry and high power (>50W) pumping methods on thermal lensing should be performed to develop a method for the reduction of thermal lensing in Yb:KYW crystals.

Bibliography (or References)

[1] L. F. Johnson, J. E. Geusic and L. G. Van Uitert, "Coherent Oscillations From Tm+3, Ho3+, Yb^{3+} and Er^{3+} Ions in Yttrium Aluminium Garnet,"," *Appl. Phys. Lett,* vol. 7, pp. 127-129, 1965.

[2] R. M. Kolbas, N. G. Anderson, W. D. Laidig, Y. Sin, Y. C. Lo, K. Y. Hsieh and Y. J. Yang, "Strained-layer InGaAs-GaAs-AIGaAs photopumped and current injection lasers," *IEEE J. Quantum Electron.,* vol. 24, pp. 1605-1613, 1988.

[3] R. Niu, J. Liu, C. Liu, Y. Liu and L. Qin, "Theoretical investigation on thermal lensing effects of Yb:$KY(WO_4)_2$ in diode-pumped lasers," *Optik,* vol. 122, pp. 1931-1934, 2011.

[4] M. Hildebrandt, U. Bünting, U. Kosch, D. Haussmann, T. Levy, M. Krause, O. Müller, B. Bartuch and W. Viöl, "Diode-pumped Yb:KYW thin-disk laser operation with wavelength tuning to small quantum defects," *Optics Communications,* vol. 259, no. 2, pp. 796-798, 2006.

[5] S. Chenais , F. Balembois, F. Druon, G. Lucas-Leclin and P. Georges, "Thermal lensing in diode-pumped ytterbium lasers-Part I: theoretical analysis and wavefront measurements," *IEEE J. Quantum Electron.,* vol. 40, no. 9, pp. 1217-1234, 2004.

[6] A. Y. Cabezas, L. G. Komai and R. P. Treat, "Dynamic measurements of phase shifts in laser amplifiers," *Appl. Opt. ,* vol. 5, pp. 647-651, 1966.

[7] D. Mudge, M. Ostermeyer, P. J. Veitch, J. Munch, B. Middlemiss, D. J. Ottaway and M. W. Hamilton, "Power scalable TEM_{00} CW Nd:YAG laser with thermal lens compensation," *Selected Topics in Quantum Electronics, IEEE Journal of,* vol. 6, no. 4, pp. 643-649, 2000.

[8] C. Pfistner, R. Weber, H. P. Weber, S. Merazzi and R. Gruber, "Thermal beam distortions in end-pumped Nd:YAG, Nd:GSGG, and Nd:YLF rods," *Quantum Electronics, IEEE Journal of,* vol. 30, no. 7, pp. 1605-1615, 1994.

[9] J. L. Blows, J. M. Dawes and T. Omatsu, "Thermal lensing measurements in line-focus end-pumped neodymium yttrium aluminium garnet using holographic lateral shearing interferometry," *J. Appl. Phys. ,* vol. 83, p. 2901, 1998.

[10] V. Magni, "Multielement stable resonators containing a variable lens," *J. Opt. Soc. Am. A,*

vol. 4, no. 10, pp. 1962-1969, 1987.

[11] L. D. DeLoach, S. A. Payne, L. L. Chase, L. K. Smith, W. L. Kway and W. F. Krupke, "Evaluation of absorption and emission properties of Yb^{3+} doped crystals for laser applications," *IEEE J. Quantum Electron.,* vol. 29, p. 1179 , 1993.

[12] F. Träger, Handbook of lasers and optics, Springer, 2007.

[13] N. V. Kuleshov, A. A. Lagatsky, A. V. Podlipensky, V. P. Mikhailov and G. Huber, "Pulsed laser operation of Y b-dope d $KY(WO_4)_2$ and $KGd(WO_4)_2$," *Opt. Lett.,* vol. 22, pp. 1317-1319, 1997.

[14] W. F. Krupke, "Ytterbium solid-state lasers. The first decade," *Selected Topics in Quantum Electronics, IEEE Journal of,* vol. 6, no. 6, pp. 1287-1296, 2000.

[15] R. Paschotta, J. Nilsson, A. C. Tropper and D. C. Hanna, "Ytterbium-doped fiber amplifiers," *Quantum Electronics, IEEE Journal of,* vol. 33, no. 7, pp. 1049-1056, 1997.

[16] D. C. Hanna, R. M. Percival, I. R. Perry, R. G. Smart, P. J. Suni, J. E. Townsend and A. C. Tropper, "Continuous-wave oscillation of a monomode ytterbium-doped fibre laser," *Electronics Letters,* vol. 24, no. 17, pp. 1111-1113, 1988.

[17] H. M. Pask, R. J. Carman, D. C. Hanna, A. C. Tropper, C. J. Mackechnie, P. R. Barber and J. M. Dawes, "Ytterbium-doped silica fiber lasers: versatile sources for the 1-1.2 μm region," *Selected Topics in Quantum Electronics, IEEE Journal of,* vol. 1, no. 1, pp. 2-13, 1995.

[18] D. Y. Shen, J. K. Sahu and W. A. Clarkson, "Highly efficient Er,Yb-doped fiber laser with 188W free-running and > 100W tunable output power," *Opt. Express,* vol. 13, pp. 4916-4921, 2005.

[19] A. S. Grabtchikov, A. N. Kuzmin, V. A. Lisinetskii, V. A. Orlovich, A. A. Demidovich, M. B. Danailov, H. J. Eichler, A. Bednarkiewicz, W. Strek and A. N. Titov, "Laser operation and Raman self-frequency conversion in Yb:KYW microchip laser," *Applied Physics B,* vol. 75, no. 6-7, pp. 795-797, 2002.

[20] A. A. Kaminskii, P. V. Klevtsov and A. A. Pavlyuk, "Stimulated emission from $KY(WO_4)_2$: Nd^{3+} crystal laser," *Phys. Status Solidi A,* vol. 5, no. 2, pp. K79-K81, 1971.

[21] A. A. Kaminskii, A. F. Konstantinova, V. P. Orekhova, A. V. Butashin, R. F. Klevtsova and A. A. Pavlyuk, "Optical and nonlinear laser properties of the $\chi(3)$-active monoclinic α-

$KY(WO_4)_2$ crystals," *Crystallogr. Rep.* , vol. 46, no. 4, pp. 665-672, 2001.

[22] J. E. Hellström, B. Jacobsson, V. Pasiskevicius and F. Laurell, "Quasi-two-level Yb:KYW laser with a volume Bragg grating," *Opt. Express* , vol. 15, pp. 13930-13935, 2007.

[23] S. A. Payne, L. L. Chase, H. W. Newkirk, L. K. Smith and W. F. Krupke, "$LiCaAlF_6:Cr^{3+}$: a promising new solid-state laser material," *IEEE Journal of Quantum Electronics,* vol. 24, no. 11, pp. 2243-2252, 1988.

[24] A. Brenier, "A new evaluation of Yb^{3+}-doped crystals for laser applications," *Journal of Luminescence,* vol. 92, no. 3, pp. 199-204, 2001.

[25] Y. E. Romanyuk, C. N. Borca, M. Pollnau, S. Rivier, V. Petrov and U. Griebner, "Yb-doped $KY(WO_4)_2$ planar waveguide laser," *Opt. Lett.*, vol. 31, pp. 53-55, 2006.

[26] P. A. Loiko, V. V. Filippov, K. V. Yumashev, N. V. Kuleshov and A. A. Pavlyuk, "Thermo-optic coefficients study in $KGd(WO_4)_2$ and $KY(WO_4)_2$ by a modified minimum deviation method," *Appl. Opt.* , vol. 51, pp. 2951-2957 , 2012.

[27] V. V. Filippov and I. T. Bodnar, "Thermo-optical parameters and dispersion of pure and Yb^{3+}-doped $KY(WO_4)_2$ laser crystals," *Appl. Optics,* vol. 46, pp. 6843-6846, 2007.

[28] V. V. Filippov, N. V. Kuleshov and I. T. Bodnar, "Negative thermo-optical coefficients and athermal directions in monoclinic $KGd(WO_4)_2$ and $KY(WO_4)_2$ laser host crystals in the visible region," *Appl. Phys. B,* vol. 87, no. 4, pp. 611-614, 2007.

[29] K. V. Yumashev, N. N. Posnov, P. V. Prokoshin, V. L. Kalashnikov, F. Mejid, I. G. Poloyko, V. P. Mikhailov and V. P. Kozich, "Z-scan measurements of nonlinear refraction and Kerr-lens mode-locking with Yb^{3+}:$KY(WO_4)_2$," *Optical and Quantum Electronics,* vol. 32, no. 1, pp. 43-48, 2000.

[30] A. I. Vodchits, V. P. Kozich, V. A. Orlovich and P. A. Apanasevich, "Z-Scan studies of KYW, KYbW, KGW, and $Ba(NO_3)_2$ crystals," *Optics Communications,* vol. 263, no. 2, pp. 304-308, 2006.

[31] N. Thilmann, G. Strömqvist, M. C. Pujol, V. Pasiskevicius, V. Petrov and F. Díaz, "Nonlinear refractive indices in Yb^{3+}-doped and undoped monoclinic double tungstates $KRE(WO_4)_2$ where RE=Gd, Y, Yb, Lu," *Applied Physics B: Lasers & Optics,* vol. 96, no. 2/3, p. 385, 2009.

[32] P. A. Loiko, K. V. Yumashev, N. V. Kuleshov, G. E. Rachkovskaya and A. A. Pavlyuk, "Detailed characterization of thermal expansion tensor in monoclinic $KRe(WO_4)_2$ (where Re= Gd, Y, Lu, Yb)," *Optical Materials,* vol. 34, no. 1, pp. 23-26, 2011.

[33] P. A. Loiko, K. V. Yumashev, N. V. Kuleshov and A. A. Pavlyuk, "Thermo-optical properties of pure and Yb-doped monoclinic $KY(WO_4)_2$ crystals," *Applied Physics B,* vol. 106, no. 3, pp. 663-668, 2012.

[34] M. C. Pujol, X. Mateos, R. Solé, J. Massons, J. Gavaldà, F. Díaz and M. Aguilo, "Linear thermal expansion tensor in $KRE(WO_4)_2$ (RE = Gd, Y, Er, Yb) monoclinic crystals," *Mater. Sci. Forum* , Vols. 378-381, pp. 710-715, 2001.

[35] R. L. Aggarwal, D. J. Ripin, J. R. Ochoa and T. Y. Fan, "Measurement of thermo-optic properties of $Y_3Al_5O_{12}$, $Lu_3Al_5O_{12}$, $YAIO_3$, $LiYF_4$, $LiLuF_4$, BaY_2F_8, $KGd(WO_4)_2$, and $KY(WO_4)_2$ laser crystals in the 80–300 K temperature range," *J. Appl. Phys,* vol. 98, no. 2005, p. 103514.

[36] K. Petermann, D. Fagundes-Peters, J. Johannsen, M. Mond, V. Peters, J. J. Romero, S. Kutovoi, J. Speiser and A. Giesen, "Highly Yb-doped oxides for thin-disc lasers," *Journal of Crystal Growth,* vol. 275, no. 1-2, pp. 135-140, 2005.

[37] S. Biswal, S. P. O'Connor and S. R. Bowman, "Thermo-optical parameters measured in ytterbium-doped potassium gadolinium tungstate," *Appl. Opt.* , vol. 44, pp. 3093-3097, 2005.

[38] Ò. Silvestre, J. Grau, M. C. Pujol, J. Massons, M. Aguiló, F. Díaz, M. T. Borowiec, A. Szewczyk, M. U. Gutowska, M. Massot, A. Salazar and V. Petrov, "Thermal properties of monoclinic $KLu(WO_4)_2$ as a promising solid state laser host," *Opt. Express* , vol. 16, pp. 5022-5034, 2008.

[39] M. M. Mazur, F. A. Kuznetsov, L. I. Mazur, A. A. Pavlyuk and V. I. Pustovoit, "Elastic and Photoelastic Properties of $KY(WO_4)_2$ Single Crystals," *Inorganic Materials,* vol. 48, no. 1, pp. 67-73, 2012.

[40] A. A. Demidovich, A. N. Kuzmin, G. I. Ryabtsev, M. B. Danailov, W. Strek and A. N. Titov, "Influence of Yb concentration on Yb:KYW laser properties," *Journal of Alloys and Compounds,* Vols. 300-301, pp. 238-241, 2000.

[41] P. Klopp, V. Petrov, U. Griebner and G. Erbert, "Passively mode-locked Yb:KYW laser

pumped by a tapered diode laser," *Opt. Express* , vol. 10, pp. 108-113, 2002.

[42] N. V. Kuleshov, A. A. Lagatsky, V. G. Shcherbitsky, V. P. Mikhailov, E. Heumann, T. Jensen, A. Diening and G. Huber, "CW laser performance of Yb and Er,Yb doped tungstates," *Appl. Phys. B,* vol. 64, no. 4, pp. 409-413, 1997.

[43] P. Moulton, "Paramagnetic ion lasers," in *Handbook of Laser Science and Technology, M. J. Weber, Ed.* , Boca Raton, FL, CRC, 1983, p. 211.

[44] A. R. Reinberg, L. A. Riseberg, R. M. Brown, R. W. Wacker and W. C. Holton, "GaAs: Si LED pumped Yb-doped YAG laser," *Appl. Phys. Lett.,* vol. 19, p. 11, 1971.

[45] A. Lagatsky, C. Brown and W. Sibbett, "Highly efficient and low threshold diode-pumped Kerr-lens mode-locked Yb:KYW laser," *Opt. Express,* vol. 12, pp. 3928-3933, 2004.

[46] S. Erhard, J. Gao, A. Giesen, A. Contag, A. A. Lagatsky, A. Abdolvand, N. V. Kuleshov, J. Aus der Au, G. J. Spuhler, F. Brunner, R. Paschotta and U. Keller, "High power Yb:KGW and Yb:KYW thin disk laser operation," *Lasers and Electro-Optics, 2001. CLEO '01. Technical Digest. Summaries of papers presented at the Conference on,* pp. 333-334, 2001.

[47] A. L. Calendron, K. S. Wentsch and M. J. Lederer, "High power cw and mode-locked oscillators based on Yb:KYW multi-crystal resonators," *Opt. Express* , vol. 16, pp. 18838-18843 , 2008.

[48] G. H. Kim, G. H. Yang, D. S. Lee, A. V. Kulik, E. G. Sall', S. A. Chizhov, V. E. Yashin and U. Kang, "High-power efficient cw and pulsed lasers based on bulk Yb : KYW crystals with end diode pumping," *Quantum Electron.* , vol. 42, p. 292, 2012.

[49] B. Jacobsson, J. Hellström, V. Pasiskevicius and F. Laurell, "Widely tunable Yb:KYW laser with a volume Bragg grating," *Opt. Express,* vol. 15, pp. 1003-1010, 2007.

[50] B. Jacobsson, J. E. Hellström, V. Pasiskevicius and F. Laurell, "Tunable Yb:KYW laser using volume Bragg grating in s-polarization," *Appl. Phys. B,* vol. 91, pp. 85-88, 2008.

[51] K. Seger, B. Jacobsson, V. Pasiskevicius and F. Laurell, "Tunable Yb:KYW laser using a transversely chirped volume Bragg grating," *Opt. Express* , vol. 17, pp. 2341-2347 , 2009.

[52] Y. Kalisky, O. Kalisky, U. Rachum, G. Boulon and A. Brenier, "Comparative performance of passively Q-Switched diode-pumped Yb^{3+}-doped tungstate and garnet lasers using Cr^{4+}:YAG saturable absorber," *Selected Topics in Quantum Electronics, IEEE Journal of,*

vol. 13, no. 3, pp. 502-510, 2007.

[53] F. M. Bain, A. A. Lagatsky, S. V. Kurilchick, V. E. Kisel, S. A. Guretsky, A. M. Luginets, N. A. Kalanda, I. M. Kolesova, N. V. Kuleshov, W. Sibbett and C. T. A. Brown, "Continuous-wave and Q-switched operation of a compact, diode-pumped Yb^{3+}:$KY(WO_4)_2$ planar waveguide laser," *Opt. Express* , vol. 17, pp. 1666-1670, 2009.

[54] H. Liu, J. Nees and G. Mourou, "Diode-pumped Kerr-lens mode-locked Yb:$KY(WO_4)_2$ laser," *Opt. Lett.* , vol. 26, pp. 1723-1725, 2001.

[55] F. Brunner, T. Südmeyer, E. Innerhofer, F. Morier-Genoud, R. Paschotta, V. E. Kisel, V. G. Shcherbitsky, N. V. Kuleshov, J. Gao, K. Contag, A. Giesen and U. Keller, "240-fs pulses with 22-W average power from a mode-locked thin-disk Yb:$KY(WO_4)_2$ laser," *Opt. Lett.* , vol. 27, pp. 1162-11164, 2002.

[56] T. C. Schratwieser, C. G. Leburn and D. T. Reid, "Highly efficient 1 GHz repetition-frequency femtosecond Yb^{3+}:$KY(WO_4)_2$ laser," *Opt. Lett.* , vol. 37, pp. 1133-1135, 2012.

[57] M. Endo, A. Ozawa and Y. Kobayashi, "Kerr-lens mode-locked Yb:KYW laser at 4.6-GHz repetition rate," *Opt. Express* , vol. 20, pp. 12191-12197 , 2012.

[58] A. Schmidt, S. Rivier, W. B. Cho, J. H. Yim, S. Y. Choi, S. Lee, F. Rotermund, D. Rytz, G. Steinmeyer, V. Petrov and U. Griebner, "Sub-100 fs single-walled carbon nanotube saturable absorber mode-locked Yb-laser operation near 1 μm," *Opt. Express* , vol. 17, pp. 20109-20116 , 2009.

[59] A. Killi, A. Steinmann, J. Dörring, U. Morgner, M. J. Lederer, D. Kopf and C. Fallnich, "High-peak-power pulses from a cavity-dumped Yb:$KY(WO_4)_2$ oscillator," *Opt. Lett.*, vol. 30, pp. 1891-1893, 2005.

[60] A. Beyertt, D. Nickel and A. Giesen, "Femtosecond thin disk Yb:KYW regenerative amplifier," *Appl. Phys. B* , vol. 80, no. 6, pp. 655-660, 2005.

[61] M. Larionov, F. Butze, D. Nickel and A. Giesen, "Femtosecond thin disk Yb:KYW regenerative amplifier with astigmatism compensation," in *Advanced Solid-State Photonics,* Vancouver, Canada, paper WB11, 2007.

[62] C. L. Li, X. H. Zhang, G. Y. Jin, W. Liang, J. Q. Lin and Y. Dong, "All-solid-state Yb:KYW-LBO blue-green laser at 500 nm," *Laser Physics,* vol. 21, no. 6, pp. 1028-1030,

2011.

[63] M. Jacquemet, F. Druon, F. Balembois and P. Georges, "Single-frequency operation of diode-pumped Yb:KYW at 1003.4 nm and 501.7 nm by intracavity second harmonic generation," *Appl. Phys. B* , vol. 85, pp. 69-72, 2006.

[64] S. A. Meyer, J. A. Squier and S. A. Diddams, "Diode-pumped Yb:KYW femtosecond laser frequency comb with stabilized carrier-envelope offset frequency," *The European Physical Journal D,* vol. 48, no. 1, pp. 19-26, 2008.

[65] B. E. A. Saleh and M. C. Teich, Fundamentals of Photonics, 2nd Edition, Wiley, 2007.

[66] *LAS-CAD GmbH,* Munich.

[67] I. V. Mochalov, "Laser and nonlinear properties of the potassium gadolinium tungstate laser crystal $KGd(WO_4)_2:Nd^{3+}$-(KGW:Nd)," *Opt. Eng.*, vol. 36, no. 6, pp. 1660-1669, 1997.

[68] P. A. Loiko, K. V. Yumashev, N. V. Kuleshov, G. E. Rachkovskaya and A. A. Pavlyuk, "Thermo-optic dispersion formulas for monoclinic double tungstates $KRe(WO_4)_2$ where Re = Gd, Y, Lu, Yb," *Optical Materials,* vol. 33, no. 11, pp. 1688-1694, 2011.